# The Calcium-independent Transient Outward Potassium Current in Isolated Ferret Right Ventricular Myocytes

## *I. Basic Characterization and Kinetic Analysis*

DONALD L. CAMPBELL, RANDALL L. RASMUSSON, YUSHENG QU, and HAROLD C. STRAUSS

From the Departments of Pharmacology, Biomedical Engineering, and Medicine, Duke University Medical Center, Durham, North Carolina 27710

ABSTRACT Enzymatically isolated myocytes from ferret right ventricles (12–16 wk, male) were studied using the whole cell patch clamp technique. The macroscopic properties of a transient outward $K^+$ current $I_{to}$ were quantified. $I_{to}$ is selective for $K^+$, with a $P_{Na}/P_K$ of 0.082. Activation of $I_{to}$ is a voltage-dependent process, with both activation and inactivation being independent of $Na^+$ or $Ca^{2+}$ influx. Steady-state inactivation is well described by a single Boltzmann relationship ($V_{1/2} = -13.5$ mV; $k = 5.6$ mV). Substantial inactivation can occur during a subthreshold depolarization without any measurable macroscopic current. Both development of and recovery from inactivation are well described by single exponential processes. Ensemble averages of single $I_{to}$ channel currents recorded in cell-attached patches reproduce macroscopic $I_{to}$ and indicate that inactivation is complete at depolarized potentials. The overall inactivation/recovery time constant curve has a bell-shaped potential dependence that peaks between $-10$ and $-20$ mV, with time constants (22°C) ranging from 23 ms ($-90$ mV) to 304 ms ($-10$ mV). Steady-state activation displays a sigmoidal dependence on membrane potential, with a net aggregate half-activation potential of +22.5 mV. Activation kinetics (0 to +70 mV, 22°C) are rapid, with $I_{to}$ peaking in ~5–15 ms at +50 mV. Experiments conducted at reduced temperatures (12°C) demonstrate that activation occurs with a time delay. A nonlinear least-squares analysis indicates that three closed kinetic states are necessary and sufficient to model activation. Derived time constants of activation (22°C) ranged from 10 ms (+10 mV) to 2 ms (+70 mV). Within the framework of Hodgkin-Huxley formalism, $I_{to}$ gating can be described using an $a^3i$ formulation.

Address reprint requests to Dr. Donald L. Campbell, Department of Pharmacology, Duke University Medical Center, Box 3845, Durham, NC 27710.

J. GEN. PHYSIOL. © The Rockefeller University Press · 0022-1295/93/04/0571/31 $2.00
Volume 101 April 1993 571–601

## INTRODUCTION

Potassium ($K^+$) currents are fundamentally important in initiating and modulating repolarization of the cardiac action potential (for reviews see Hondeghem and Snyders, 1990; Hume, Uehara, Hadley, and Harvey, 1990; Pennefather and Cohen, 1990; Gintant, Cohen, Datyner, and Kline, 1991). An inactivating $K^+$ current that has been described in many cardiac tissues is the so-called "transient outward $K^+$ current" or $I_{to}$ (e.g., Binah, 1990; Gintant et al., 1991). Despite important quantitative kinetic differences, $I_{to}$ in cardiac muscle appears to be qualitatively similar to the inactivating $K^+$ current $I_A$ present in many neuronal cell types (e.g., Connor and Stevens, 1971; Neher, 1971; Adams, Smith, and Thompson, 1980; Rudy, 1988).

$I_{to}$ has been postulated to modulate phase 1 repolarization and frequency-dependent changes in action potential configuration, and to contribute to differences in action potential configuration between different regions of the heart (atrium, Purkinje fiber, ventricle), endocardium versus epicardium, and young versus adult human atrial fibers (reviewed in Binah, 1990). Although $I_{to}$ plays a key role in cardiac repolarization, its basic properties have not been fully characterized. For example, there are contradictory reports about its gating, pharmacological, and neuromodulatory characteristics, and the number and magnitude of current components comprising total $I_{to}$ in any given cardiac myocyte type are uncertain (i.e., a voltage-activated, $Ca^{2+}$-independent $I_{to,1}$ and a $Ca^{2+}$-activated $I_{to,2}$; see, for example, Callewaert, Vereecke, and Carmeliet, 1986; Escande, Coulombe, Faivre, Deroubaix, and Coraboeuf, 1987; Bendorf, 1988; Giles and Imaizumi, 1988; Hiraoka and Kawano, 1989; Tseng and Hoffman, 1989; for review see Binah, 1990; Gintant et al., 1991). To date, no complete quantitative kinetic model of cardiac $I_{to}$ has been developed, particularly in regard to activation kinetics. In this article we analyze the macroscopic $Ca^{2+}$-independent $I_{to}$ ($I_{to,1}$) in single myocytes that have been enzymatically isolated from ferret right ventricles, and we describe and quantify its selectivity characteristics and potential-dependent macroscopic gating kinetics (activation and inactivation/recovery). In the accompanying article (Campbell, Qu, Rasmusson, and Strauss, 1993), we describe a kinetic model of state-dependent block of $Ca^{2+}$-independent $I_{to}$ by 4-aminopyridine (4-AP) which is based in part on the kinetic analysis presented here.

Preliminary accounts of this work have appeared in abstract form (Campbell, Qu, Rasmusson, and Strauss, 1991*a*, *b*).

## METHODS

### *Myocyte Isolation*

10–16-wk-old male ferrets (Marshall Farms, North Rose, NY) were anesthetized by intraperitoneal injection of sodium pentobarbital. Hearts were excised and perfused via the aorta on a Langendorff perfusion apparatus at 37°C. Perfusion solutions were bubbled with 100% $O_2$, and perfusion pressure was maintained at ~70 cm $H_2O$. Initial perfusion (5–10 min) with solution I, composed of (mM) 144 NaCl, 0.4 $NaH_2PO_4$, 5.4 KCl, 1 $MgCl_2$, 2.5 $CaCl_2$, 5.6 glucose, and 10 HEPES, pH 7.25, was followed by a 5-min perfusion with solution II (solution I with no added $Ca^{2+}$ and 100 μM EGTA, 3.5 mM $MgCl_2$, 20 mM taurine, and 10 mM creatine), followed by a final 12–15-min perfusion with solution III (solution II with EGTA removed and 100 μM $CaCl_2$ added) containing 1 mg/ml collagenase (either type I or type II; Worthington Biochemical

Corp., Freehold, NJ), 0.1–0.2 mg/ml protease (type XIV; Sigma Chemical Co., St. Louis, MO), and 0.05 mg/ml elastase (type II-A; Sigma Chemical Co.). The right ventricle was dissected free, placed in fresh enzyme solution II containing an additional 10 mg/ml bovine serum albumin (essentially fatty acid free; Sigma Chemical Co.), and spun gently at 37°C. Aliquots of solution II were collected at 10-min intervals, filtered through course nylon mesh, and centrifuged (~1,000 *g* for 1 min). Myocyte pellets were then directly resuspended in tissue culture media (Medium 199; Sigma Chemical Co.; $[CaCl_2]$ = 1.8 mM) supplemented with 10% fetal calf serum and 1% antibiotics and stored at room temperature until used. All experiments were conducted within 8–12 h after initial myocyte isolation.

### *Electrophysiological Techniques*

Myocytes were studied (Axopatch 1-C amplifier; Axon Instruments, Inc., Foster City, CA) using the single microelectrode gigaseal patch clamp technique in the whole cell recording configuration (Hamill, Marty, Neher, Sakmann, and Sigworth, 1981; Marty and Neher, 1983). Electrodes were fabricated from borosilicate glass tubing (TW150F-4, 1.5 mm o.d.; World Precision Instruments, Inc., Sarasota, FL) using a two-stage pipette puller (L/M-3P-A; Adams & List Associates, Ltd., Westbury, NY) and heat polished to a tip diameter of ~1 μm. When filled with recording solution (described below), resistances were 2–4 MΩ. Cells were pipetted into a small (~0.5 ml) recording chamber mounted on a modified stage (Adams & List Associates, Ltd.) of an inverted microscope (Nikon Diaphot) and were perfused at 1–4 ml/min. Tip potentials were typically −5 mV or less; no corrections for offset potentials were applied. After gigaseal formation (>30–50 GΩ), the whole cell recording configuration was achieved by applying a brief (0.1–10 ms) 1.5-V zap pulse to rupture the patch. 10–15 min elapsed before experimental recordings to allow stabilization (e.g., Marty and Neher, 1983). All experiments were conducted at room temperature (21–23°C) or lower (11–13°C).

For whole cell recording of $I_{to}$, patch pipettes contained the following intracellular solution (mM): 140 KCl, 1 $MgCl_2$, 5 EGTA, 5 ATP (Mg salt), 5 $Na_2$-creatinephosphate, 0.2 GTP, and 10 HEPES, pH 7.40. Myocytes were initially perfused with a normal $Na^+$-containing extracellular solution (mM): 144 NaCl, 5.4 KCl, 1 $MgCl_2$, 2.5 $CaCl_2$, 5.6 glucose, and 10 HEPES, pH 7.40. Seals were formed and action potentials were recorded in this solution. Unless otherwise specified, measurements were conducted during perfusion of a completely $Na^+$-free $I_{to}$ solution (144 mM *N*-methyl-D-glucamine-Cl [NMDG-Cl], 5.4 mM KCl, 1 mM $MgCl_2$, 2.5 mM $CaCl_2$, 12–20 × $10^{-6}$ M tetrodotoxin [TTX], 500 × $10^{-6}$ M $CdCl_2$, and 10 mM HEPES, pH 7.40) to eliminate $I_{Na}$, $I_{Ca}$, the $Na^+/Ca^{2+}$ exchanger current (e.g., Campbell, Giles, Robinson, and Shibata, 1988), and any possible $Na^+$-activated $K^+$ currents (e.g., Sanguinetti, 1990; Dukes and Morad, 1991). Because we have observed (Qu, Y., and D. L. Campbell, unpublished observations) that concentrations of nitrendipine required to completely block $I_{Ca}$ (1–10 μM) also block $I_{to}$ (see also Gotoh, Imaizumi, Watanabe, Shibata, Clark, and Giles, 1991; Lefevre, Coulombe, and Coraboeuf, 1991), we used 500 μM $Cd^{2+}$ to block $I_{Ca}$.

To determine the ionic selectivity characteristics of $I_{to}$, the apparent reversal potential, $E_{rev}$, of deactivating $I_{to}$ tail currents was measured in solutions containing both $Na^+$ and $K^+$. In these experiments, the concentration of TTX was increased to 50–60 μM, and $[KCl]_o$ was varied from 1 to 100 mM, keeping the total $[NaCl]_o$ + $[KCl]_o$ constant at 149.4 mM. Only $E_{rev}$ measurements from myocytes in which 50–60 μM TTX adequately suppressed $I_{Na}$ were used for analysis.

Two additional $K^+$ currents were observed upon initial establishment of the whole cell configuration: (*a*) a background, inwardly rectifying current, $I_{K1}$, and (*b*) a very slowly activating, delayed rectifier–type current, $I_{KDR}$. As described for other cardiac myocyte types (e.g., Harvey and Ten Eick, 1988; Gintant et al., 1991), $I_{K1}$ was instantaneous and displayed a typical, highly nonlinear current–voltage (*I-V*) relationship (see Fig. 1 *B*), which made application of conven-

tional linear leakage subtraction protocols impossible. However, $I_{K1}$ does not contribute appreciable current in the range of potentials where $I_{to}$ activates in ferret ventricular myocytes. Activation of $I_{KDR}$ in these myocytes is extremely slow compared with the kinetics of $I_{to}$ at 22°C, with half-activation times typically longer than ~2–4 s. $I_{KDR}$ is also typically less than ~15% of peak $I_{to}$ immediately after establishment of the whole cell configuration, and cooling the myocytes to 10–12°C markedly delayed the onset and further reduced the magnitude of $I_{KDR}$. Furthermore, during the initial 10–15 min stabilization time, $I_{KDR}$ progressively declined and, in most myocytes, was nearly or completely eliminated, presumably due to exchange of the pipette solution with the cytosol (cf. Duchatelle-Gourdon, Hartzell, and Lagrutta, 1988; Wasserstrom and Ten Eick, 1991). Only recordings in which $I_{KDR}$ had completely run down were used. In all cases, the initial 10–15-min perfusion did not affect the magnitude or time course of $I_{to}$. Therefore, all of our recordings were obtained from myocytes that had been perfused with control intracellular solution and thus were not necessarily subject to the full complement of cellular regulatory mechanisms.

For single-channel measurements, patch pipettes were manufactured from Corning 7052 glass (1.5 mM o.d., 0.86 mM i.d.; A-M Systems, Inc., Everett, WA), heat polished, and coated with Sylgard (Dow Corning Corp., Midland, MI). Tip resistances were 8–12 MΩ. Patch pipettes were filled with either normal NMDG-Cl, 5.4 KCl solution, or 144 NaCl, 5.4 KCl $E_{rev}$ solution (described above). Channel activity was recorded in the cell-attached configuration at 22°C; myocytes were bathed in either physiological 144 NaCl, 5.4 KCl $E_{rev}$ solution or an isotonic KCl solution (144 mM KCl, 5.4 NaCl, 1 $MgCl_2$, 1 EGTA, and 10 HEPES, pH 7.40) to zero the membrane potential. Averages of blank records at each potential were used to subtract capacitive transients and the background seal resistance leak current.

### *Data Analysis and Fitting Procedures*

Current traces and clamp pulses were recorded on video tape using a four-channel A/D VCR adaptor (PCM 4; Medical Systems Corp., Greenvale, NY). Whole cell currents were filtered (8-pole Bessel) at 2–5 kHz, while single-channel recordings were filtered at 1 kHz. Data were digitized off-line using a 125 kHz A/D board (Labmaster TL-1 DMA; Scientific Solutions Inc., Solon, OH) in a 386 personal computer running pClamp software (Axon Instruments Inc.). Data analysis utilized both commercially available software (pClamp, Lotus, FigP) and customized programs. Simulations were carried out using a fourth-order, variable step size, Runge-Kutta algorithm written in double precision FORTRAN.

In experiments designed to quantitate activation, bath temperature was reduced to ~12°C to separate more reliably activation kinetics from the capacitive current transients ($I_{cap}$). To minimize further contamination from $I_{cap}$, the membrane potential was first stepped to a potential at which macroscopic $I_{to}$ did not activate (typically −20 mV; see Fig. 1 *B*). The resulting $I_{cap}$ was then linearly scaled and subtracted from current records elicited at more depolarized potentials.

During the capacitive transient ($I_{cap} = C_m * dV/dt$) the membrane potential is not clamped but is approaching its final value with a characteristic time constant ($\tau \approx R_{series} * C_m$). Therefore, for each subtracted record $I_{cap}$ was analyzed separately to determine the time required for it to decline 90% from its initial peak value. This 90% rise time for membrane potential was then taken as time zero for all subsequent analyses and fits of activation kinetics. In other words, the $I_{cap}$-subtracted records were not analyzed back to the immediate on of the voltage clamp pulse, but were fit only once the membrane potential was within 10% of its final value. No attempt was made to fit current time courses before this time.

The subtracted current traces at 12°C were fit using an equation of the form:

$$A * (1 - \exp[B * t])^n * \exp(C * t) + R \quad (1)$$

where $A$ is an amplitude scalar, $B$ and $C$ are the aggregate rate constants ($1/[\alpha + \beta]$) of activation and inactivation, respectively, $n$ is the activation power, $t$ is time, and $R$ is steady-state current (Hodgkin and Huxley, 1952). Initial fits were obtained using a Marquardt nonlinear least-squares method where $A$, $B$, $C$, $n$, and $R$ were all allowed to vary freely to determine the mean value of $n$. Subtracted data obtained at both 12 and 22°C were then fit to the same equation, but the value of $n$ was fixed to the mean value previously determined at 12°C. The extracted time constants were then combined with measured steady-state data to derive first-order rate constants for activation. Apparent $Q_{10}$ values for the fully activated *I-V* relationship and for activation and inactivation rate constants were then calculated from mean values obtained from fits using the mean fixed $n$ value.

Possible limitations of the fitting procedures used in our analysis of $I_{to}$ activation kinetics are described in Appendix II.

## RESULTS

### *Basic Observations*

Action potentials recorded from ferret right ventricular myocytes in physiological 144 mM $Na^+$ saline (Fig. 1 *A*) typically show a 4-AP-sensitive early phase of repolarization (i.e., phase 1) immediately before the plateau, suggesting the presence of a rapidly activating outward current. Fig. 1 *B* shows current recordings from a myocyte bathed in $Na^+$-free NMDG solution elicited by voltage clamp pulses applied from a holding

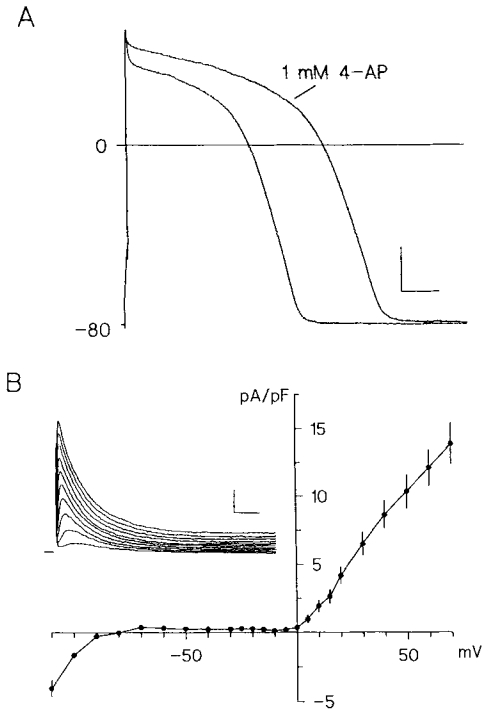


FIGURE 1. (*A*) Ferret right ventricular myocyte action potentials recorded from a normal 144 mM $Na^+$ saline before and after application of 1 mM 4-AP (current clamp conditions, HP = −80 mV, 4-ms depolarizing current pulses applied at 0.125 Hz). Note the presence of a 4-AP-sensitive rapid phase 1 repolarization preceding the plateau. Calibration: 60 ms, 20 mV. (*B*) Representative transient outward currents (*inset*) and peak *I-V* relationship obtained in $Na^+$-free NMDG saline. (*Inset*) Currents elicited in response to 500-ms voltage clamp pulses from +10 to +100 mV in 10-mV increments (frequency = 0.2 Hz, HP = −70 mV). Main figure shows the mean peak *I-V* relationship (expressed as current density) obtained from six myocytes in NMDG saline. (Mean absolute current at +50 mV, 979 ± 126 pA; mean capacitance, 103.9 ± 21.4 pF ± SD). Calibration: 40 ms, 600 pA.

potential (HP) of −70 mV to test potentials from +10 to +100 mV. The outward current elicited upon depolarization displays rapid activation and inactivation. Our experimental conditions indicate that activation of this current is not dependent on the influx of either $Na^+$ or $Ca^{2+}$. The main panel of Fig. 1 shows the peak *I-V* relationship obtained from six myocytes in NMDG solution over the range −110 to +70 mV. The peak *I-V* is approximately linear from 0 to +70 mV.

The outward current illustrated in Fig. 1 declines with maintained depolarization, possibly due to (*a*) channel inactivation, (*b*) simultaneous activation of a second inward current, or (*c*) depletion and/or accumulation of ions near the surface membrane (e.g., in sarcolemmal caveolae; Gabella, 1978). To demonstrate that the decline is due to channel inactivation, as well as to determine if the current is due to a single conductance mechanism, a series of envelope-of-tails tests was conducted (e.g., Hodgkin and Huxley, 1952; Hume, Giles, Robinson, Shibata, Nathan, Kanai, and Rasmusson, 1986; Sanguinetti and Jurkiewicz, 1990). The basic protocol is illustrated in the inset in Fig. 2. From HP = −70 mV a variable duration depolarizing

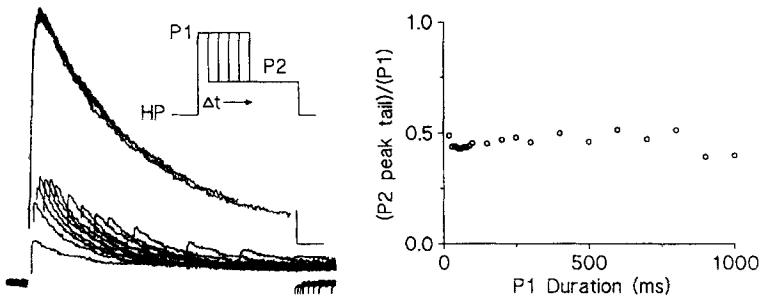


FIGURE 2. Representative envelope-of-tails test at 12°C. Voltage clamp protocol illustrated in the inset (P1 = +50 mV for increasing durations *t* of 10 ms and greater, P2 = −10 mV, HP = −70 mV). The current during P1 was measured immediately before P2 repolarization. The steady-state value of the P1 current was subtracted from the measured current to give an activated P1(*t*) current amplitude. Similarly, the steady-state current value of the P2 tail current was subtracted from the peak tail current to give an estimated P2 tail current amplitude. The ratio of the subtracted currents (P2 tail/P1(*t*)) remains constant during the entire voltage clamp protocol. Calibration: 100 ms, 100 pA.

pulse, P1, was applied to +50 mV to activate the current. The membrane potential was then stepped to a fixed hyperpolarized potential, P2, to generate a deactivating tail current. The duration of P1 was then progressively increased to generate a waveform or envelope of tail currents. If the decline of the outward current is due to inactivation of a single current component, then the ratio of peak tail currents during P2 to currents at the immediate end of P1 should remain constant. To enhance resolution of the tail currents during both the rapid rising phase of activation as well as the slower phase of decline, bath temperature was reduced (~12°C) to slow channel kinetics. The envelope-of-tails test illustrated in Fig. 2 (P2 = −10 mV) shows that the ratio remains constant with increasing P1 duration, suggesting that the decline of the current is due neither to changes in selectivity nor to accumulation/

depletion of ions, but rather to changes in membrane conductance. Similar results (12°C) were obtained from three additional myocytes.

The ionic selectivity of this current was determined in various $Na^+$-containing solutions in which the $[KCl]_o$ was varied and $[NaCl]_o$ + $[KCl]_o$ was kept constant at 149.4 mM (see Methods). From HP = −70 or −80 mV a brief 10–20-ms depolarizing P1 pulse was applied (generally to +70 mV), followed by a P2 pulse to progressively hyperpolarized potentials (10-mV increments) to determine $E_{rev}$ of the tail currents. $E_{rev}$ varied from −59.0 ± 3.5 mV (in 1 mM $[KCl]_o$, 148.4 mM $[NaCl]_o$ saline) to −4.2 ± 2.5 mV (in 100 mM $[KCl]_o$, 49.4 mM $[NaCl]_o$ saline) (Fig. 3). The extrapolated $E_{rev}$ was dependent on $[K^+]_o$ and was well described by the Goldman-Hodgkin-Katz constant field voltage equation (Goldman, 1943; Hodgkin and Katz, 1949) with a $P_{Na}/P_K$ of 0.082 (see Table I). Fig. 3 compares the predicted $E_{rev}$ derived

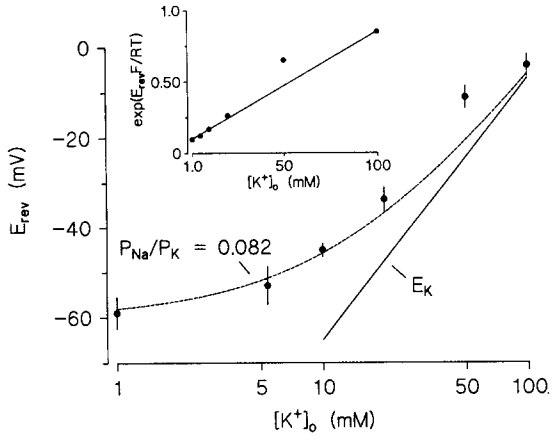


FIGURE 3. Mean reversal potential, $E_{rev}$, of transient outward current tail currents as a function of $[K^+]_o$. $E_{rev}$ was measured in $Na^+$-containing solutions ($[KCl]_o$ + $[NaCl]_o$ kept constant at 149.4 mM, TTX 50–60 μM; see Methods). (*Inset*) Linear transformation and fit to the mean $E_{rev}$ data points using the Goldman-Hodgkin-Katz constant field voltage equation. Extrapolated parameters: $[K^+]_i$ = 132.8 mM; $P_{Na}/P_K$ = 0.082. Main figure shows $E_{rev}$ measured as a function of $[K^+]_o$. The solid straight line is the theoretically predicted Nernst $K^+$ equilibrium potential $E_K$. The dashed curve is the fit to the measured $E_{rev}$ data points using the constant field voltage equation and the extrapolated parameters. Data points are mean (±SD) of $n$ = 4–5 myocytes at each $[KCl]_o$, except 50 mM $[KCl]_o$, where $n$ = 2.

from the constant field equation ($P_{Na}/P_K$ = 0.082) with the experimental $E_{rev}$ data. Since only $Na^+$ and $K^+$ were varied, it is clear that the current is selective for $K^+$ and that it is not a $Cl^-$ current. Furthermore, complete replacement of extracellular 144 mM NMDG-Cl by NMDG-methanesulfonate (MSA) did not abolish this transient outward current.

Additional experiments indicate that this current can be reduced or blocked by 4-AP (see Campbell et al., 1993), 10–20 μM quinidine (Qu, Y., and D. L. Campbell, unpublished data; cf. Imaizumi and Giles, 1987), and external and internal $Cs^+$. We therefore term this current $I_{to}$ for transient outward $K^+$ current following terminology previously introduced (e.g., Clark, Giles, and Imaizumi, 1988; Giles and Imaizumi, 1988; Binah, 1990; Gintant et al., 1991).

*Quantitative Kinetic Analysis of $I_{to}$*

INACTIVATION CHARACTERISTICS

The envelope-of-tails data (Fig. 2) in combination with the $E_{rev}$ data (Fig. 3) confirm that $I_{to}$ is due to a time-dependent change in membrane $K^+$ conductance, which subsequently inactivates to a final level. However, at 500–800 ms an outwardly rectifying component of steady-state current was observed. It is important to recall that the currents illustrated have not been leakage corrected. When the scaled capacitive current was subtracted (see Methods), the instantaneous (time zero) current changes after a depolarizing pulse were identical to the steady-state currents measured at the end of the pulse. The average value of the residual current at the end of depolarizing pulses relative to the instantaneous time zero current was $-2.1 \pm 1.7\%$ ($\pm$ SE; $n = 6$ myocytes), expressed as a percentage of peak. Therefore, the maximum value for the residual, noninactivated component is 0.34%, using a $P = 0.01$ criterion for rejection. Thus, the outwardly rectifying current component appears to be a time-independent, background current. This indicates that $I_{to}$ completely inactivates at depolarized potentials and that the residual current at the end of the test pulse is composed of a time-independent or instantaneous background leak current.

Additional experiments demonstrated that this instantaneous background leak current is sensitive to extracellular $Cl^-$ concentration. For example, complete replacement of 144 mM NMDG-Cl by NMDG-MSA significantly reduced the magnitude of the current at the end of 500-ms depolarizing clamp pulses (e.g., 59 ± 6% [SD] reduction at +50 mV; $n = 3$ myocytes). However, extracellular $Cl^-$ replacement with NMDG-MSA did not alter the time-to-peak, kinetics of inactivation, or magnitude of the transient $I_{to}$ (i.e., $I_{to,peak} - I_{500\ ms}$) over the depolarized range of potentials (+20 to +100 mV). These results indicate that this $Cl^-$ conductance is indeed acting as a time-independent, background leak conductance, with properties very similar to the background $Cl^-$ conductance recently described in canine atrial myocytes by Sorota (1992). In our macroscopic kinetic analysis of $I_{to}$ we have therefore included appropriate corrections for this background current.

*Steady-state inactivation.* The potential dependence of the steady-state inactivation relationship, $i_\infty$, of macroscopic $I_{to}$ was determined using a conventional, double-pulse inactivation voltage clamp protocol (see Fig. 4 *A*, *inset*). From a fixed holding potential (−70 or −80 mV), 800-ms P1 pulses were applied in 10-mV increments, followed by a fixed 500-ms P2 pulse to +50 mV (frequency = 0.125 Hz). As shown in Fig. 4 *A*, as P1 became increasingly depolarized, $I_{to}$ during P2 progressively declined, with complete inactivation occurring at +10 mV for the myocyte illustrated. Applying hyperpolarizing P1 pulses down to −110 mV did not further increase control $I_{to}$ during P2. The $i_\infty$ relationship was constructed from the normalized ratio (peak P2 $I_{to} - I_{500\ ms}$)/(control P2 $I_{to} - I_{500\ ms}$) plotted as a function of P1 potential, where $I_{500\ ms}$ is the background current at the end of the 500-ms P2 pulse. The $i_\infty$ relationship obtained from seven myocytes in control NMDG saline is shown in Fig. 4 *B*. Increasing P1 to 1,500 ms did not alter this relationship (data not shown). From this curve it is apparent that substantial inactivation of $I_{to}$ occurs at potentials well hyperpolarized to the threshold for channel opening (Fig. 1 *B*). The

inactivation relationship observed in normal 144 mM $Na^+$, 50 μM TTX solution (in which adequate suppression of $I_{Na}$ was obtained; $n$ = 3 myocytes) was identical to that observed in NMDG solution.

*Kinetics of $I_{to}$ inactivation and recovery.* Complete description of the kinetics of $I_{to}$ inactivation and recovery from inactivation required three different voltage clamp protocols: (*a*) direct fit analysis of the inactivating phase of $I_{to}$ at depolarized

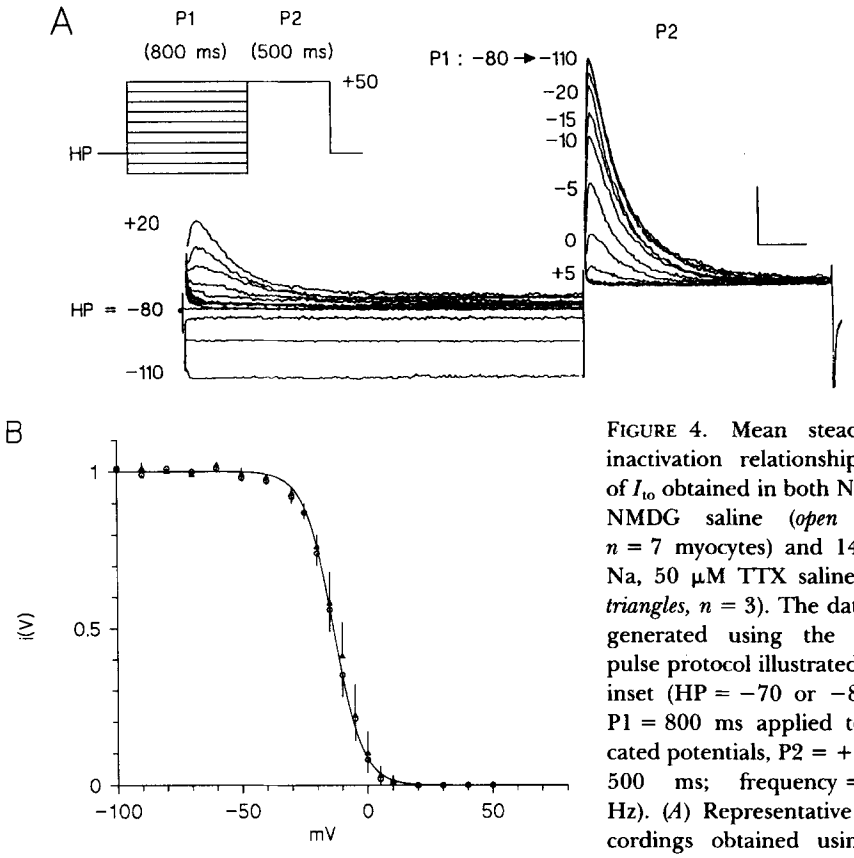


FIGURE 4. Mean steady-state inactivation relationship $i_\infty(V)$ of $I_{to}$ obtained in both $Na^+$-free NMDG saline (*open circles*, $n$ = 7 myocytes) and 144 mM Na, 50 μM TTX saline (*filled triangles*, $n$ = 3). The data were generated using the double pulse protocol illustrated in the inset (HP = −70 or −80 mV, P1 = 800 ms applied to indicated potentials, P2 = +50 mV, 500 ms; frequency = 0.125 Hz). (*A*) Representative $I_{to}$ recordings obtained using this protocol for the P1 potentials indicated. Calibration: 100 ms, 200 pA. (*B*) Mean $I_{to}$ steady-state inactivation relationship obtained using the protocol described in *A*. Data were fit (*solid curve*) with a Boltzmann relationship ($i_\infty(V) = 1/[1 + \exp([V_{1/2} - V]/k)$, where $V_{1/2}$ = −13.5 mV and $k$ = 5.65 mV.

potentials (~0 or +10 to +70 mV); (*b*) modified double-pulse analysis of development of inactivation in the range of potentials where marked inactivation of $I_{to}$ occurs but little or no open channel current is observed (−20 to approximately +10 mV; c.f. DeCoursey, 1990); and (*c*) recovery from inactivation in the hyperpolarized range of potentials where inactivation is either minimal or does not develop (−30 to −90 mV).

(*i*) Direct fit analysis of inactivation. Direct fit analysis of $I_{to}$ indicated that inactivation (500–800-ms clamp pulses) was well described by a single exponential

process (Fig. 5). The mean inactivation time constants, $\tau_i$, derived by direct fit analysis at 22°C were relatively rapid (e.g., 46.5 ± 10.1 ms, +50 mV). The mean direct fit $\tau_i$ values as a function of membrane potential (0 to +70 mV) are illustrated in Fig. 10 *A* (open triangles). $\tau_i$ was essentially potential insensitive in the range of +20 to +70 mV.

To validate the assumptions underlying our macroscopic current analysis, we examined the ensemble average inactivation behavior of single $I_{to}$ channels recorded in the cell-attached configuration. Less than 10% of the patches contained $I_{to}$ channel activity (although nearly every patch displayed $I_{K1}$ channel activity in response to hyperpolarizing pulses). Typically, the minimum number of $I_{to}$ channels per successful patch was two or three. Fig. 6 *A* shows results obtained from one cell-attached patch that contained at least two $I_{to}$ channels. In this experiment the patch pipette contained 144 mM NaCl and 5.4 mM KCl solution (see Methods), and the myocyte

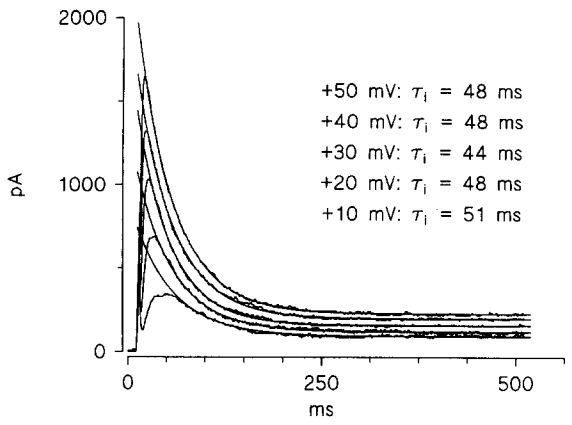


FIGURE 5. Kinetics of inactivation of conducting $I_{to}$ channels. Representative direct fit analysis of $I_{to}$ inactivation in response to 500-ms voltage clamp pulses applied from +10 to +50 mV (HP = −70 mV, frequency = 0.125 Hz). The smooth solid curves show single exponential fits to the inactivating phase of $I_{to}$, with the best-fit inactivation time constant $\tau_i(V)$ indicated for each potential. The potential dependence (0 to +70 mV) of the mean inactivation time constants obtained using direct fit analysis is given in Fig. 10 *A* (*open triangles*).

was perfused with the same solution. Representative channel behavior at an applied patch potential of +120 mV (i.e., 120 mV depolarized relative to the resting potential; c.f. Clark et al., 1988) is illustrated for selected recordings. The channel is small in amplitude and displays very rapid, flickering behavior. The single-channel *I-V* relationship obtained for this patch is shown in Fig. 6 *B*. The estimated single-channel conductance was ~4 pS and gave an extrapolated reversal potential of $V_{applied}$ = +19 mV. Assuming a resting potential of −70 to −75 mV (i.e., the values that we typically recorded upon attainment of the whole cell configuration), this extrapolated $E_{rev}$ compares well with our macroscopic measurements under the same conditions ($E_{rev}$ = −55 mV; Fig. 3). During the 500-ms depolarizing pulses, channels activated very near the beginning of the pulse, displayed rapid, flickering, bursting behavior before finally closing, and then typically remained closed for the duration of the pulse. Ensemble averages of 100 consecutive 500-ms traces at $V_{applied}$ = +120, +140, and +160 mV were obtained from this patch (Fig. 6 *C*). The ensemble average

at all three applied potentials rapidly activated and then inactivated. Inactivation was well described as a single exponential process, with time constants that were independent of pulse potential.

We also examined single-channel kinetics under conditions mimicking those used to isolate $I_{to}$ (patch pipette: 144 mM NMDG-Cl, 5.4 mM KCl solution; cell bathed in isotonic KCl solution; see Methods). Ensemble averages (Fig. 7) obtained over the depolarized range of potentials from cell-attached patches containing at least two

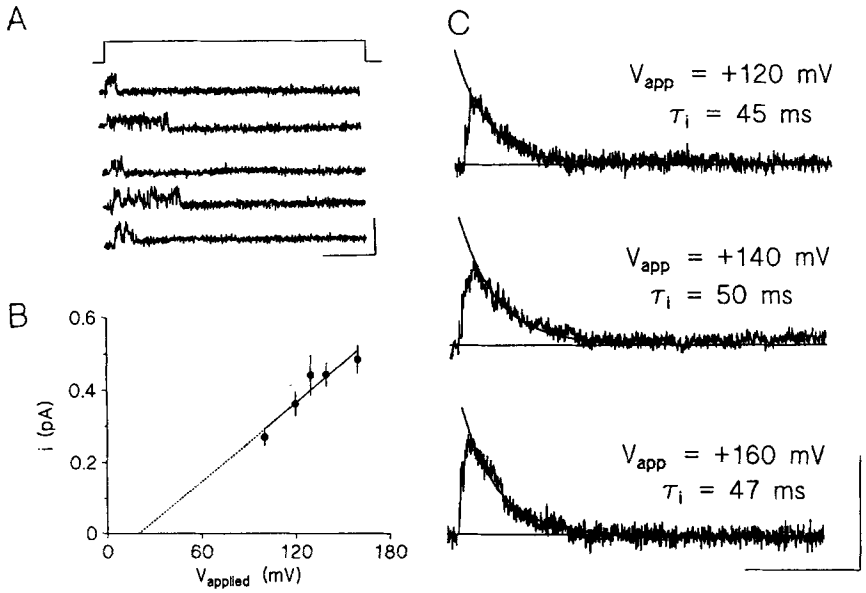


FIGURE 6. Single $I_{to}$ channel behavior. Patch pipette and myocyte bathing solutions: 144 mM NaCl, 5.4 mM KCl solution (see Methods). (*A*) Unitary currents in response to an applied potential of +120 mV. Assuming a resting potential of −70 to −75 mV, this would correspond to +50 mV. This patch contained more than one channel; for clarity of presentation, the records shown were selected where single channel events did not overlap. Calibration: 100 ms, 1 pA. (*B*) Single channel *I-V* relationship measured from the same patch. Data points are means (±SD) of 8–20 events at each applied potential. The straight line gives an extrapolated $E_{rev}$ of +19 mV applied, which corresponds to a transmembrane $E_{rev}$ of approximately −50 to −55 mV. (*C*) Ensemble averages from the same patch. Averages were constructed from 100 consecutive traces at each potential. The solid curves are single exponential fits to inactivation with indicated time constants. Data were filtered at 1 kHz and digitized at 400 μs/point. Calibration: 150 ms, 0.25 pA.

channels rapidly activated and then inactivated and were similar to those obtained in normal $Na^+$ saline. Inactivation was again well described by a single exponential process with potential-independent time constants.

When ensemble average currents were analyzed statistically, the average value of the residual current during the last 50 ms of the depolarizing pulses relative to the baseline holding current was 4.28 ± 1.0% (±SE) expressed as percentage of peak. Therefore, the maximal value for a residual, noninactivating component of $I_{to}$ is

5.5%, using a $P = 0.01$ criterion for rejection. Within the limits of the cell-attached patch configuration (i.e., accuracy of subtracting blank records to eliminate both capacitive transients and leak current), the data indicate that $I_{to}$ completely inactivates at depolarized potentials.

The ensemble average behavior of single channels in cell-attached patches closely reconstructs the macroscopic behavior of $I_{to}$ recorded in the whole cell configuration. These results, which suggest that $I_{to}$ is due to a single type of $K^+$ channel that rapidly activates and then completely inactivates in the depolarized range of potentials, support the validity of the macroscopic techniques (to be described below) used for detailed analysis.

(*ii*) Development of inactivation of nonconducting $I_{to}$ channels. A modified double P1-P2 protocol was used to determine the kinetics of development of inactivation over the range −20 to +10 mV. A constant P2 (+50 mV, 500 ms) was immediately

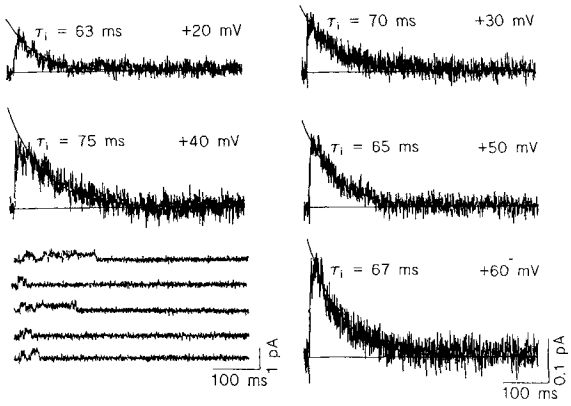


FIGURE 7. Single exponential fits to ensembles of single $I_{to}$ channels under recording conditions designed to mimic those used for the macroscopic analysis. Patch pipette: 144 mM NMDG-Cl, 5.4 mM KCl saline; bath: isotonic KCl saline (see Methods). Ensemble averages of 120 consecutive 500-ms traces at each potential. This patch contained at least two channels. Time constants of inactivation (millisecond) as indicated. The selected single-channel recordings were obtained at +40 mV. Data were filtered at 1 kHz and digitized at 400 μs/point.

preceded by a variable duration P1 to a fixed potential (−20 to +10 mV). P1 duration was then progressively increased, and the reduction of P2 $I_{to}$ as a function of P1 duration was analyzed. A representative result from this protocol for P1 = −10 and 0 mV is shown in Fig. 8. For both P1 = −10 and P1 = 0 mV, no net outward $I_{to}$ was activated, yet reduction of peak $I_{to}$ was observed during P2. In both cases inactivation developed with a single exponential time course, and the measured time constants were dependent on the P1 potential. The summarized kinetics of development of inactivation of nonconducting $I_{to}$ channels obtained using this protocol are given in Fig. 10*A* (filled diamonds). The largest time constants were obtained for P1 = −20 mV (297.1 ± 44.6 ms) and −10 mV (304.2 ± 45.7 ms). Fig. 10*A* shows that these inactivation time constants are continuous with those obtained from direct fit analysis and that they become slower with hyperpolarization (cf. DeCoursey, 1990). These results suggest that $I_{to}$ can inactivate without entering the final open and conducting state. However, conclusive demonstration of direct closed-to-inactivated

state transitions will require conditional probability analysis of twin-pulse, single-channel recordings.

(*iii*) Recovery from inactivation. The potential dependence of the kinetics of recovery from inactivation was measured using a double-pulse P1-P2 protocol: both P1 and P2 were stepped to +50 mV for 500 ms from a fixed holding potential (−30 to −90 mV), and the interpulse interval ($\Delta t$) between P1 and P2 was progressively increased. Recovery (i.e., relative P2 current) was then determined as a function of $\Delta t$ (Fig. 9). This P1-P2 protocol was then repeated at different holding potentials. Recovery was relatively rapid and well described in most myocytes by a single exponential process. Time constants were potential dependent and decreased

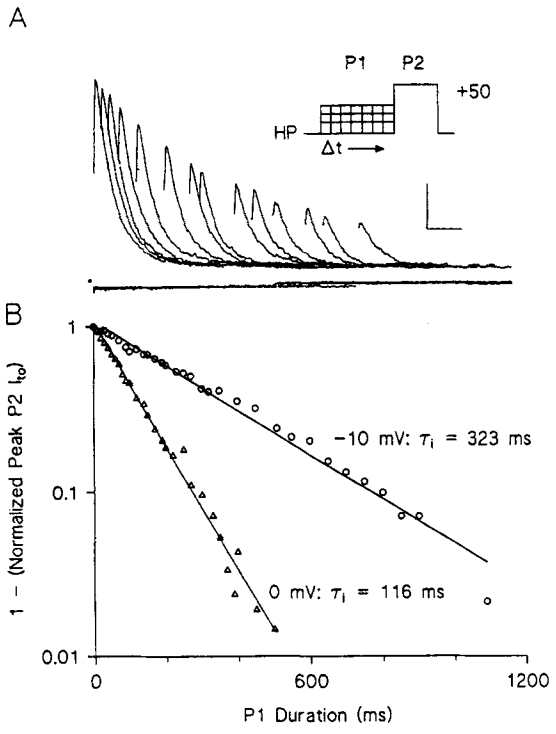


FIGURE 8. Kinetics of development of $I_{to}$ inactivation in the membrane potential range where $I_{to}$ measurably inactivates but does not conduct (−20 to +10 mV). (*A*) The double pulse P1-P2 protocol is schematically illustrated in the inset. The main figure shows the initial time course of the P2 $I_{to}$ waveform obtained from a myocyte for P1 = −10 mV. Note that the P2 $I_{to}$ progressively inactivates with increasing P1 duration, even though no measurable $I_{to}$ is activated during the P1 at −10 mV. Calibration: 100 ms, 100 pA. (*B*) Single exponential fits for development of inactivation of the P2 $I_{to}$ waveform obtained from the same myocyte for P1 = −10 and 0 mV. The potential dependence (−20 to +10 mV) of the mean time constants obtained using this protocol are given in Fig. 10 *A* (*filled diamonds*).

systematically with hyperpolarization (range: 23.5 ± 8.1 ms at −90 mV to 152.4 ± 24.0 ms at −30 mV). The complete voltage dependence (−30 to −90 mV) of the recovery time constants is given in Fig. 10 *A* (open circles).

*Summary of $I_{to}$ inactivation/recovery kinetics.* The complete kinetics of $I_{to}$ inactivation/recovery are summarized in Fig. 10. The mean $\tau_i(V)$ curve is bell shaped and peaks between −10 and −20 mV (Fig. 10 *A*), which is consistent with the experimentally measured steady-state inactivation curve $i_\infty(V)$ ($V_{1/2}$ = −13.5 mV; Fig. 4 *B*). The mean rate constant (= $1/\tau_i(V)$) curve is given in Fig. 10 *B*. The equations for the opening $\alpha_i(V)$ and closing $\beta_i(V)$ rate constants ($s^{-1}$) are given in Table I. Fig. 10 *C* shows the model predicted $i_\infty(V)$ relationship (= $\alpha_i(V)/[\alpha_i(V) + \beta_i(V)]$) plotted over

the measured steady-state inactivation data (Fig. 4 *B*). The derived $\alpha_i(V)$ and $\beta_i(V)$ values are exponentially behaved in the region of half-inactivation and accurately reproduce the experimentally measured $i_\infty(V)$ and $\tau_i(V)$ relationships.

ACTIVATION CHARACTERISTICS

*Steady-state activation.* The voltage dependence of steady-state activation was determined using a double-pulse tail current protocol: brief (5–15 ms) P1 voltage clamp pulses to progressively more depolarized potentials (10-mV steps) were

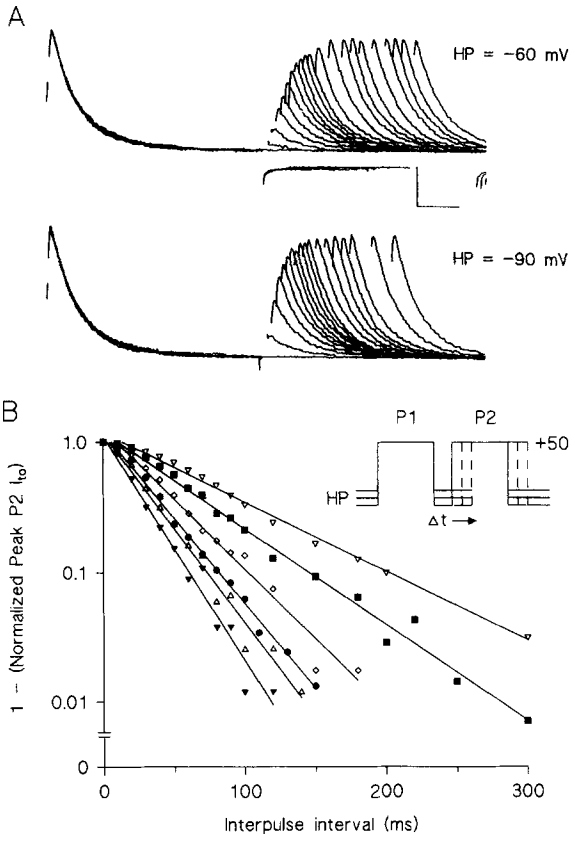


FIGURE 9. Kinetics of $I_{to}$ recovery from inactivation. (*A*) Representative $I_{to}$ recovery waveforms obtained at HP = −60 and −90 mV using the double pulse protocol illustrated in the inset in *B* (frequency = 0.125 Hz; interpulse interval *t* progressively increased, initial value 10 ms). Calibration (both traces): 100 ms, 200 pA. (*B*) Voltage dependence of kinetics of recovery for the myocyte illustrated in *A* over the HP range −40 to −90 mV. Semilogarithmically transformed data fit with single exponential time constants of recovery as follows: HP = −90 mV (*filled inverted triangles*), 25 ms; −80 (*open triangles*), 30 ms; −70 (*filled circles*), 33 ms; −60 (*open diamonds*), 40 ms; −50 (*filled squares*), 59 ms; −40 (*open inverted triangles*), 82 ms. The potential dependence (−30 to −90 mV) of the mean time constants of $I_{to}$ recovery are given in Fig. 10 *A* (*open circles*).

immediately followed by P2 pulses to a fixed hyperpolarized potential where $I_{to}$ was not activated (typically −20 mV; see schematic inset in Fig. 11). The peak P2 tail currents give a measure of the instantaneous conductance of $I_{to}$ activated during P1($V$). Normalizing the peak P2 tail currents as a function of P1($V$) measures the steady-state potential dependence of the aggregate activation process $a_\infty(V)^n$ = (P2 $I_{to}$ tail)/(maximal P2 $I_{to}$ tail), where $n$ is the activation power (an integer value). As illustrated in the inset of Fig. 11, the peak tail currents measured during P2 saturate above +50 mV. The main body of Fig. 11 shows the mean $I_{to}$ steady-state activation

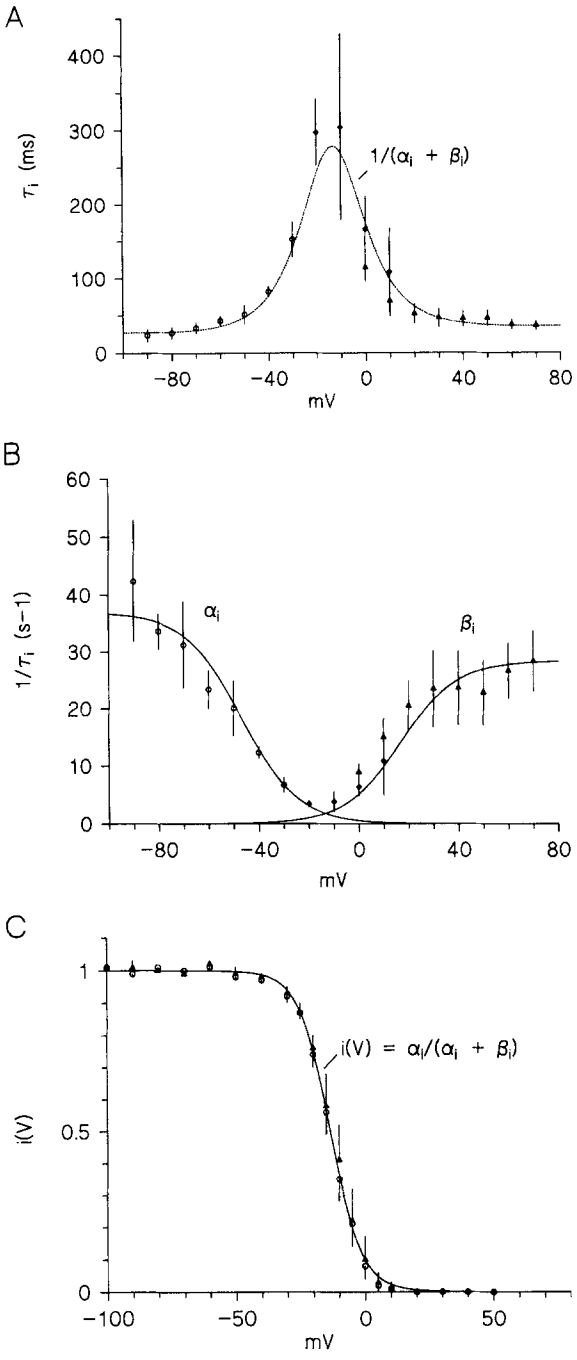


FIGURE 10. Overall potential dependence of $I_{to}$ inactivation/recovery kinetics. (*A*) Mean $\tau_i(V)$ relationship obtained using the protocols described in Figs. 5, 8, and 9. *Circles*, recovery; *filled diamonds*, development of inactivation; *triangles*, direct fits. (Data points are mean ± SD at each potential of: recovery, $n$ = 5–6 myocytes; development of inactivation, $n$ = 4 myocytes; direct fit inactivation, $n$ = 12–16 myocytes.) The smooth bell-shaped curve is the theoretical fit to the mean $\tau_i(V)$ data points using the derived rate constants for inactivation $\alpha_i(V)$ and $\beta_i(V)$ illustrated in *B*. (*B*) Voltage dependence of inactivation rate constants $\alpha_i(V)$ and $\beta_i(V)$ obtained from analysis of the reciprocal inactivation time constant curve (i.e., $1/\tau_i(V)$) illustrated in *A*. Smooth curves are fits to the data points using the $\alpha_i$ and $\beta_i$ equations given in Table I. (*C*) Theoretically predicted steady-state inactivation relationship $i_\infty(V)$ $(= \alpha_i(V)/[\alpha_i(V) + \beta_i(V)])$ calculated using the derived $\alpha_i(V)$ and $\beta_i(V)$ values illustrated in *B*. The overlayed data points are from Fig. 4 *B*.

relationship. $a^n$ saturates by +50 mV and has a half-activation potential $V_h$ of +22.5 mV.

*Kinetics of $I_{to}$ activation.* To resolve reliably the kinetics of activation, measurements were conducted at both 12 and 22°C in the same myocyte. Cooling to 12°C substantially slowed $I_{to}$ activation, and sigmoid activation could be observed without capacitive transient subtraction. As described in Methods, capacitive transients were subtracted and the 90% rise time was taken as time zero for the subtracted $I_{to}$ record. The mean time zero was 3.24 ± 0.27 ms (± SEM, $n$ = 6 myocytes). Currents at 12°C were initially fit using a Marquardt fitting routine to Eq. 1, where all parameters were allowed to vary freely. Fig. 12, *A* and *B*, shows fits obtained from a myocyte at 12°C for potentials of +20, +40, and +70 mV. These subtracted records indicate that $I_{to}$ activation is sigmoidal. For the myocyte illustrated, best-fit $n$ values of 2.72 for +20 mV, 2.80 for +40 mV, and 3.20 for +70 mV were obtained.

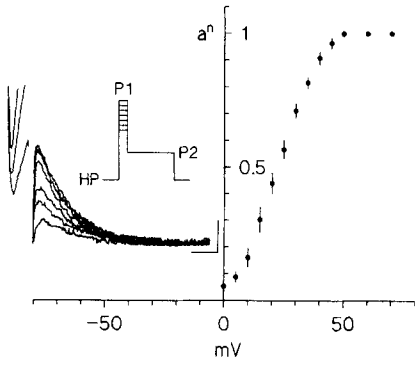


FIGURE 11. Steady-state net aggregate activation relationship $a_\infty(V)^n$ for $I_{to}$ obtained using the standard saturating tail current protocol illustrated in the inset. The inset also shows representative $I_{to}$ tail current data generated using this protocol (15 ms P1 to +15, 20, 25, 35, 40, 50, and 70 mV; P2 = −20 mV, 150 ms; HP = −70 mV) from a single myocyte. The P2 tail currents saturated above +50 mV. Calibration: 15 ms, 50 pA. The main figure shows the mean steady-state aggregate activation relationship obtained using this protocol. Half-activation of the aggregate process occurs at $V_h$ = +22.5 mV. Data points mean (±SD) of $n$ = 10–16 myocytes at each potential.

From a total of 42 determinations of $n$ conducted on $I_{to}$ recorded at 12°C, a mean value of $n$ = 3.09 ± 0.15 (± SEM) was obtained (potential range +10 to +70 mV, $n$ = 6 myocytes). We considered the case where the average value of $n$ obtained from each myocyte was assumed to be a random variable. Under this assumption, evaluation of the average $n$ values obtained from each of the six myocytes used in our analysis resulted in rejection of the null hypothesis of $n \geq 4$ ($P < 0.05$). Inclusion of the 5% error introduced by the 90% rise-time criterion (Appendix II) did not affect rejection of the hypothesis $n \geq 4$. Finally, in three additional myocytes in which the value of $n$ was determined at both HP = −70 mV and HP = −100 mV (12°C; depolarizing pulses +20 to +50 mV), we failed to observe a statistically significant increase in the value of $n$ with hyperpolarization; i.e., Cole-Moore shifts were not readily apparent over this potential range (Cole and Moore, 1960). Although

Cole-Moore shifts may be present for $I_{to}$, such shifts at very negative potentials violate the assumptions of our analysis (Appendix I). Furthermore, the transitions underlying such shifts may be too rapid to resolve and may be occurring before the establishment of voltage clamp control.

Based on this statistical analysis, and for modeling purposes, the integer value of $n$ was therefore fixed at $n = 3$. Currents at both 12 and 22°C were then refit with Eq. 1 to extract the best-fit values of the activation rate constants. Fig. 12, *C* and *D*, shows

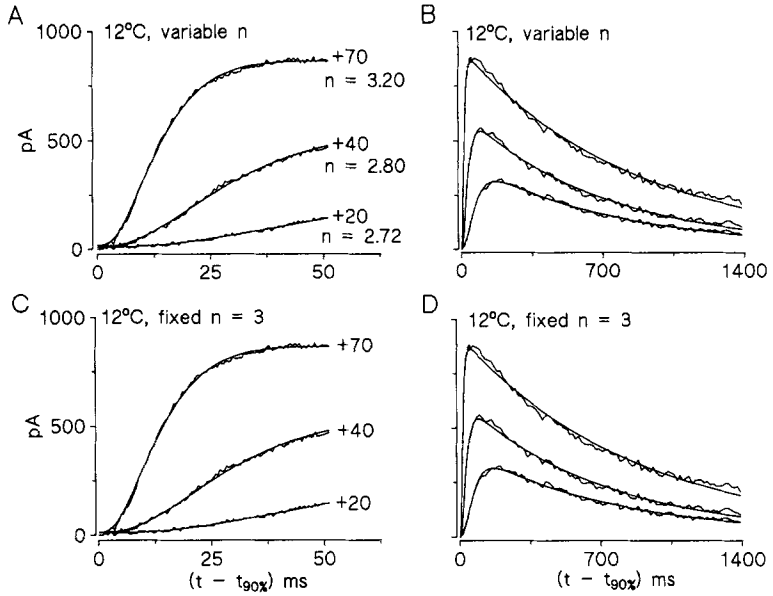


FIGURE 12. Determination of the mean value of the activation power, $n$, at 12°C. *A* and *B* show representative $I_{to}$ recordings elicited at +20, +40, and +70 mV at 12°C (*noisy traces*) overlayed with computer fits to Eq. 1, where the value of $n$ was allowed to vary freely (see Methods). Capacitive transients have been subtracted using the protocol described in the text. *A* shows the first 20 ms of the traces, while *B* shows the entire time course of the fit to the same traces so as to illustrate inactivation. Note that in accordance with the 90% rise time criterion, the time scale is given as $t - t_{90\%}$. The best-fit $n$ values obtained at each potential for this particular myocyte are indicated in *A* next to each $I_{to}$ trace. Also note from *B* that the kinetics of $I_{to}$ inactivation are greatly slowed down compared with those observed at 22°C (see Fig. 14). *C* and *D* show the same $I_{to}$ recordings and computer fits to them after fixing the value of $n = 3$.

such an analysis conducted on the current recordings at 12°C illustrated in Fig. 12, *A* and *B*. Fixing the value of $n = 3$ gives fits that are virtually indistinguishable from those where $n$ was allowed to vary freely. Kinetic analysis using $n = 3$ also produced a sigmoid delay in activation, which was consistent with $I_{to}$ recordings obtained at 22°C (Fig. 13).

*Summary of $I_{to}$ activation kinetics.* Fig. 14*A* shows the previous steady-state activation relation (Fig. 11) and the adjusted activation relationship for $n = 3$ for a

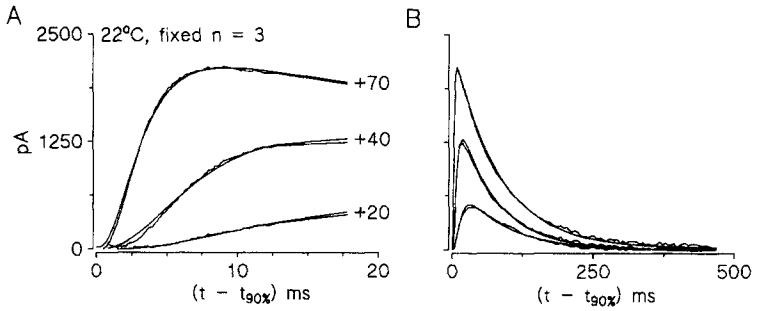


FIGURE 13. Representative fits to $I_{to}$ kinetics at +20, +40, and +70 mV at 22°C fit using Eq. 1 and a fixed value of $n = 3$ for (*A*) the first 20 ms and (*B*) the total $I_{to}$ traces so as to illustrate inactivation. Capacitive currents were subtracted; time scale is given as $t - t_{90\%}$.

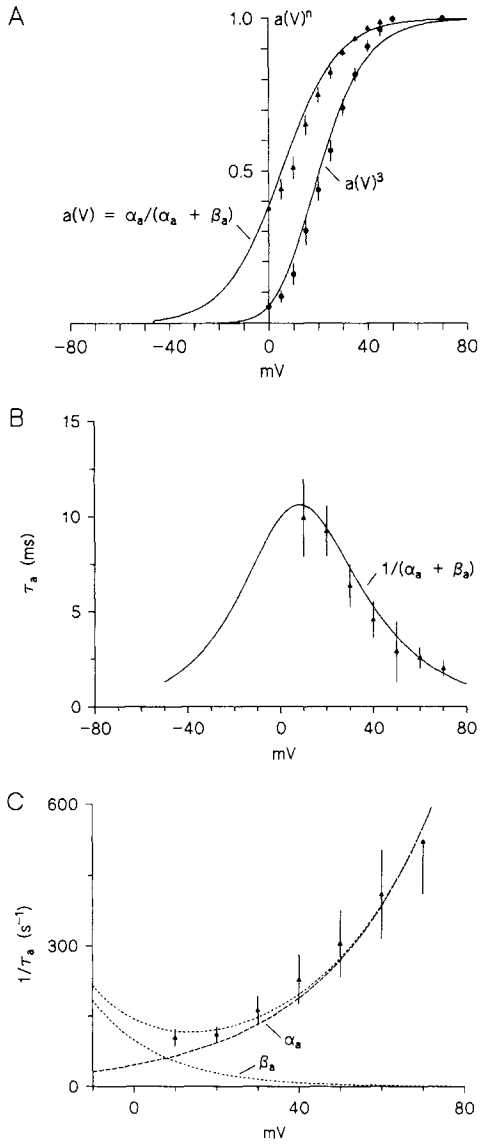


FIGURE 14. Kinetics of $I_{to}$ activation at 22°C. (*A*) Adjusted steady-state activation relationship $a_\infty(V)$. The data points labeled $a_\infty(V)^3$ (*circles*) are the previous experimentally measured points given in Fig. 11, while the data points labeled $a_\infty(V)$ (*triangles*) were generated by taking the cube root (i.e., $n = 3$) of the experimentally measured points. The smooth curve fits were generated using the $\alpha_a(V)$ and $\beta_a(V)$ values shown in *C* (i.e., $a_\infty(V) = \alpha_a(V)/[\alpha_a(V) + \beta_a(V)]$). (*B*) Voltage dependence of $I_{to}$ time constants of activation $\tau_a(V)$. The solid triangles are the mean $\tau_a(V)$ values obtained from computer fit analysis to Eq. 1 ($n = 6$ myocytes). The smooth curve fit was generated using the $\alpha_a(V)$ and $\beta_a(V)$ values illustrated in *C*. (*C*) Derived voltage dependence of the activation rate constants $\alpha_a(V)$ and $\beta_a(V)$. Data points were generated by plotting the reciprocal activation $\tau_a(V)$ data presented in *B*. The smooth curve fits were generated using the $\alpha_a(V)$ and $\beta_a(V)$ equations given in Table I.

single gating variable $a$. The adjusted relationship displays a conventional sigmoid shape and a half-activation potential of $V_h$ = +10 mV. The potential dependence (+10 to +70 mV) of the mean best-fit time constants of activation obtained at 22°C is given in Fig. 14 *B*. The values of $\tau_a(V)$ depend systemically on membrane potential, decreasing with increasing depolarization (range: 9.9 ± 2.1 ms at +10 mV to 1.9 ± 0.4 ms at +70 mV). Equations for the rate constants $\alpha_a(V)$ and $\beta_a(V)$ (Fig. 14 *C*) are given in Table I.

*Temperature dependence of $I_{to}$ gating.* The temperature dependence of the derived fully activated *I-V* relation and the mean rate constants of activation and inactivation

TABLE I

*Summary of $I_{to}$ Macroscopic Characteristics*

$I_{to} = a(V, t)^3 * i(V, t) * G_{Ito} * (V - E_{rev})$

Activation

$da(V, t)/dt = \alpha_a(V)[1 - a(V, t)] - \beta_a(V)a(V, t)$

$\alpha_a(V) = 45.16 \exp(0.03577 * V)$

$\beta_a(V) = 98.9 \exp(-0.06237 * V)$

Inactivation

$di(V, t)/dt = \alpha_i(V)[1 - i(v, t)] - \beta_i(V)i(V, t)$

$\alpha_i(V) = 1.9 \exp[-(V + 13.5)/11.3]/\{1 + 0.051335 \exp[-(V + 13.5)/11.3]\}$

$\beta_i(V) = 1.9 \exp[(V + 13.5)/11.3]/\{1 + 0.067083 \exp[(V + 13.5)/11.3]\}$

Conductance and selectivity

$G_{Ito}$ = 68.8 pS/pF at 22°C

$E_{rev} = (RT/zF) \ln(0.082[Na^+]_o + [K^+]_o)/(0.082[Na^+]_i + [K^+]_i)$

Temperature dependence (12–22°C)

$Q_{10}\, G_{Ito}$ = 1.84 ± 0.04

$Q_{10}\, \alpha_a(V)$ = 3.17 ± 0.54

$Q_{10}\, \beta_i(V)$ = 10.62 ± 0.53

Letting $V$ denote potential and $t$ time, in accordance with Hodgkin-Huxley (1952) formalism, the following abbreviations and formulations were used: $i(V, t)$, inactivation gating variable; $i_\infty(V)$, steady-state potential dependence of $i$; $\tau_i(V)$, time constant of inactivation; $\alpha_i(V)$ and $\beta_i(V)$, rate constants of inactivation (= $1/\tau_i$); $a(V, t)$, activation gating variable; $a_\infty(V)$, steady-state potential dependence of $a$; $\tau_a(V)$, time constant of activation; $\alpha_a(V)$ and $\beta_a(V)$, rate constants of activation (= $1/\tau_a$); $G_{Ito}$, maximal specific $I_{to}$ conductance; and $E_{rev}$, $I_{to}$ reversal potential. Activation has a sigmoid time dependence, which is reproduced by describing activation as being due to $n$ independent identical activation gating variables. Best-fit value of $n$ = 3. Equations: $V$ in millivolts, $t$ in seconds.

were studied at both 12 and 22°C. The mean proportional increase in parameter values for a 10°C change in temperature (referred to here for convenience as $Q_{10}$) were as follows: fully activated *I-V*, 1.84 ± 0.04; activation rate constants, 3.17 ± 0.54; and inactivation rate constants, 10.62 ± 0.53. The $Q_{10}$ value of the derived, fully activated *I-V* approximates that for open channel permeation (i.e., diffusion-limited) processes. The $Q_{10}$ value for activation also falls within the range typically reported for ionic channel activation processes. However, inactivation appears to be extremely sensitive to temperature over the range 12–22°C, slowing much more than is typically predicted.

## DISCUSSION

$I_{to}$ has been observed in mammalian cardiac myocytes enzymatically isolated from multiple regions of the heart, including crista terminalis (rabbit: Giles and van Ginneken, 1985), atrium (rabbit: Clark et al., 1988; Giles and Imaizumi, 1988; human: Escande et al., 1987; Shibata, Drury, Refsum, Aldrete, and Giles, 1989; see Sorota and Boyden, 1991), AV node (rabbit: Nakayama and Irisawa, 1985; see Billette and Giles, 1991), Purkinje fibers (sheep, cow: Callewaert et al., 1986; dog: Binah, 1990; Dangman, 1991), ventricle (mouse: Bendorf, 1988; rabbit: Hiraoka and Kawano, 1989; rat: Josephson, Sanchez-Chapula, and Brown, 1984; Apkon and Nerbonne, 1991; dog: Tseng and Hoffman, 1989; cat: Wasserstrom and Ten Eick, 1991), and possibly primary pacemaking cells of the sinoatrial node (rabbit: Nathan, 1986; Brown, Campbell, Clark, and Denyer, 1987; Denyer and Brown, 1990; see Campbell, Rasmusson, and Strauss, 1991*c*, 1992). One notable exception appears to be guinea pig ventricle, where $I_{to}$ is either absent or relatively small (e.g., Hume et al., 1990). With the possible exception of guinea pig, $I_{to}$ appears to be a nearly universal $K^+$ current system in mammalian myocardial tissue.

Our results demonstrate an $I_{to}$ in ferret right ventricular myocytes. Under our recording conditions $I_{to}$ is composed of a single $K^+$-selective current component whose activation is a conventional voltage-dependent process that does not depend on the influx of either $Na^+$ or $Ca^{2+}$. Therefore, the $I_{to}$ that we have isolated and characterized is of the $Ca^{2+}$-insensitive $I_{to,1}$ type (see Binah, 1990; Gintant et al., 1991). However, we cannot rule out the possibility that under more physiological conditions $Na^+$ and/or $Ca^{2+}$ influx could modulate $I_{to,1}$ or that $Na^+$ and/or $Ca^{2+}$ influx could activate additional currents (e.g., a $Ca^{2+}$-activated $I_{to,2}$). The properties of the calcium-insensitive $I_{to,1}$ in other cardiac myocyte types will be discussed and compared with our results. For convenience, $I_{to1}$ will be referred to simply as $I_{to}$.

### *Ionic Selectivity Characteristics of $I_{to}$*

The ionic selectivity of $I_{to}$ in ferret right ventricular myocytes is consistent with recent studies on isolated rabbit and dog myocytes in demonstrating that $I_{to}$ is a $K^+$ current (e.g., Giles and van Ginneken, 1985; Nakyama and Irisawa, 1985; Clark et al., 1988; Giles and Imaizumi, 1988; Hiraoka and Kawano, 1989; Tseng and Hoffman, 1989). Our derived $P_{Na}/P_K = 0.082$ is lower than previously reported for $I_{to}$ in other isolated mammalian cardiac myocyte types (0.11–0.26), but is similar to $P_{Na}/P_K$ values of many $K^+$ channel types (see Hille, 1992).

### *Single-Channel Studies*

Reports of single-channel properties of $I_{to}$ in cardiac muscle are somewhat limited and variable. Single $I_{to}$ channel conductances measured in the cell-attached mode (letting $[K]_p$ denote the concentration of $K^+$ in the patch pipette) of 14 pS (rabbit atrium, $[K]_p = 5$ mM: Clark et al., 1988) and 19.9 pS (rabbit AV node, $[K]_p = 5.4$ mM: Nakayama and Irisawa, 1985) have been reported. In mouse ventricular myocytes both a 27-pS and a 5-pS channel have been reported ($[K]_p = 5.4$ mM: Bendorf, 1988). The apparent unitary conductance that we have recorded in ferret right ventricular myocytes (~4–7 pS, $[K]_p = 5.4$ mM; $n = 3$) is thus in the lower

range of cardiac $K^+$ channel conductances. It is probable that some of the observed differences in conductance are due to experimental factors, such as the concentrations of cations in the patch pipette ($K^+$, $Na^+$, $Ca^{2+}$, $Mg^{2+}$). However, it also possible that in different species different $K^+$ channel types underlie the cardiac transient outward current or that different regions of the heart possess different $I_{to}$ channel subtypes. On the basis of conductance, one could speculate that the larger conductance channels observed in rabbit atrium and AV node may be more similar to *Drosophila* myotube $A_1$-type $K^+$ channels (conductances in the range of 12–16 pS, $[K]_p$ = 2 mM; e.g., Zagotta, Brainard, and Aldrich, 1988), while the lower conductance channels (mouse, ferret) may be more similar to *Drosophila* neuronal $A_2$-type $K^+$ channels (conductances in the range of 5–8 pS, $[K]_p$ = 2 mM; e.g., Solc, Zagotta, and Aldrich, 1987; Zagotta et al., 1988). We hope that these issues will be resolved as the molecular structure of various cardiac $K^+$ channels is elucidated.

Our analysis of single-channel gating characteristics is somewhat limited by the difficulties associated with measuring $I_{to}$ channel activity using the cell-attached configuration, our inability to obtain patches containing only a single $I_{to}$ channel, the relatively small size of the unitary conductance, and the very rapid flickering behavior displayed by the channels. Nonetheless, the ensemble averages have confirmed that the observed time course of macroscopic current inactivation could be accounted for at the single-channel level by a single-exponential, voltage-insensitive process. The flickering nature of the single-channel events, which appears to be a poorly resolved bursting behavior, may indicate that the channel open state may itself be a complex aggregation of very short-lived states (e.g., bursts) or subconductance levels. Nonetheless, the existence of these potential complexities does not seem to affect the overall exponential decay of the current. This is in contrast to the findings in rabbit atrial myocytes by Clark et al. (1988), who reported that the mean averaged $I_{to}$ determined from summed single-channel records inactivated as a double exponential, as did the whole cell $I_{to}$.

### *Kinetics of $I_{to}$: Inactivation/Recovery*

Inactivation of $I_{to}$ in ferret right ventricular myocytes is well described as a first-order process. The half-inactivation potential ($V_{1/2}$ = −13.5 mV) is more depolarized than that reported for several cardiac cell types; however, it is essentially identical to that reported for $I_{to}$ in isolated human atrial myocytes ($V_{1/2}$ = −14 mV; Shibata et al., 1989). Consistent with our observations, time constants of recovery from inactivation in other cardiac preparations generally appear to decrease with increasing hyperpolarization (e.g., Giles and van Ginneken, 1985; Shibata et al., 1989; Tseng and Hoffman, 1989; Binah, 1990; Gintant et al., 1991). In particular, the inactivation/recovery kinetics that we have recorded are very similar to those previously reported for $I_{to}$ in human atrial myocytes (Shibata et al., 1989). However, they differ qualitatively from the double-exponential inactivation kinetics reported for rabbit atrial (Clark et al., 1988; Giles and Imaizumi, 1988) and rat ventricular myocytes (Castle, 1992). Therefore, ferret ventricular $I_{to}$ may more closely approximate the time- and voltage-dependent characteristics of human $I_{to}$ than many other commonly studied mammalian cardiac myocytes.

*Kinetics of $I_{to}$: Activation*

In isolated mammalian cardiac myocytes it appears that only one other study has attempted to evaluate the activation power, $n$, of $I_{to}$: in rabbit crista terminalis myocytes, activation of $I_{to}$ at 20–21°C was reported to be a monoexponential process, implying $n = 1$ (Giles and van Ginneken, 1985). Apkon and Nerbonne (1991) have also analyzed activation of $I_{to}$ in rat ventricular myocytes as a single exponential process. In contrast, activation of $I_{to}$ in ferret right ventricular myocytes is distinctly nonexponential and shows a sigmoid onset. Even at 22°C, in unsubtracted records, sigmoid onset of current activation was often readily apparent in the range of potentials +10 to +30 mV. Scaled capacitive transient subtraction made this sigmoid onset apparent at most potentials. Our analysis of the sigmoidicity of $I_{to}$ activation required curve fitting of data obtained at 12°C. Thus, while the characterization of $n$ at 12°C is entirely consistent with records obtained at 22°C (compare Figs. 12 and 13), we are unable to verify this assumption directly.

It is of interest to compare the activation process of the ferret ventricular $I_{to}$ channel that we have analyzed with the recent measurements of Zagotta and Aldrich (1990) on *Shaker* $A_1$-type $K^+$ channels in cultured embryonic *Drosophila* myotubes. While the activation/inactivation sequence of the *Shaker* $A_1$-type channel appears to be more rapid at 22°C than ferret ventricular $I_{to}$, there are important qualitative similarities as well as differences in behavior between the two channel types. For example, the voltage-dependent term in the exponential portion of the activation gating variable equations are very similar (ferret right ventricle: $\alpha_a = 45.2 \exp [0.036 * V]$, $\beta_a = 91.8[-0.062 * V]$; *Shaker:* $\alpha_a = 700 \exp [0.037 * V]$, $\beta_a = 287 \exp [-0.056 * V]$). This implies that the amount of charge moved per putative activation gating particle is very similar ($Q_{ferret} = 2.5$; $Q_{Shaker} = 2.3$). However, despite this apparent similarity, our measurements indicate that the total gating charge moved per channel for ferret $I_{to}$ can be calculated to be ~7.5, while that for *Shaker* $A_1$ can be calculated to be ~9. (It should be noted that Zagotta and Aldrich [1990] rounded the total charge per gating particle down to 2, and thus calculated a total charge movement per channel of 8.) Thus, the difference in estimated total gating charge movement per channel may be difficult to distinguish between the two channel types considering the level of confidence inherent in the estimation of $Q$.

Recent advances in the studies of $K^+$ channels have revealed that the functional channel appears to be a tetramer (e.g., MacKinnon, 1991; reviewed in Miller, 1991; Jan and Jan, 1992). Given the original $n^4$ model of Hodgkin and Huxley (1952) for the delayed rectifier $K^+$ current of squid giant axon and the underlying assumption that there are four independent gating particles that must activate before the channel opens, it is tempting to generalize that the activation power $n$ should be equal to 4 in all $K^+$ channel types. In this regard, other investigators have found that a value of $n = 4$ is consistent with the sigmoidicity of activation observed for a variety of $K^+$ channels (e.g., squid axon: Hodgkin and Huxley, 1952; rat brain [RCK1] and muscle [RMK1]: Koren, Liman, Logothetis, Nadal-Ginard, and Hess, 1990; rat type II alveolar epithelial cells: DeCoursey, 1990; *Shaker* myotubes [$A_1$ type]: Zagotta and Aldrich, 1990). However, in a variety of cardiac cell types the reported best-fit activation power of various $K^+$ channel types is typically in the range of $n = 1$–2 (e.g.,

Hume et al., 1986; Pennefather and Cohen, 1990; Gintant et al., 1991). Our determination of $n = 3$ is larger than previous estimates of $n$ for other cardiac $K^+$ channel types, and is more consistent with the higher $n$ values observed for $K^+$ channels in noncardiac tissues.

Our analytically derived mean value of $n = 3$ should not be interpreted as being fundamentally inconsistent with an assumed tetrameric structure of the ferret right ventricular $I_{to}$ channel. Rather, we suggest that our data are inconsistent with the assumption of four independent processes in the activation sequence; i.e., our findings are not consistent with activation proceeding through four identical, independent, exponentially distributed processes in the activation pathway (see Vandenberg and Bezanilla [1991] for a discussion of these issues for squid axon $Na^+$ channels). In this sense, our data are consistent with recent gating current measurements of *Drosophila* wild-type *Shaker* channels expressed in *Xenopus* oocytes (Bezanilla, Perozo, Papazian, and Stefani, 1991). These gating current measurements clearly indicate that even though *Shaker* $K^+$ channels may be composed of four identical subunits, the transitions between the closed states are not equivalent. In summary, there is probably not a simple relationship between the putative number of channel subunits and the number of independent states and rate constants required to model kinetically sigmoid activation of $I_{to}$ (see also Solc and Aldrich, 1990; Zagotta and Aldrich, 1990; Bezanilla et al., 1991).

### *Potential Physiological Implications*

The activation and inactivation kinetics that we have characterized (summarized in Table I) are appropriate for $I_{to}$ to be importantly involved in generation and modulation of early phase 1 repolarization, the action potential plateau, and the early phases of action potential repolarization (cf. Giles and van Ginneken, 1985; Clark et al., 1988; Apkon and Nerbonne, 1991). Therefore, due to its overlap with the large and rapidly activating L-type calcium current, $I_{Ca,L}$, present in these myocytes (Qu, Campbell, Whorton, and Strauss, 1991; and Qu, Campbell, Himmel, and Strauss, 1992), it is possible that neuromodulation of $I_{to}$ (e.g., Apkon and Nerbonne, 1988; Braun, Fedida, Clark, and Giles, 1990; Fedida, Shimoni, and Giles, 1990) could have important effects on the excitation–contraction coupling process independent of any such effects on $I_{Ca,L}$. Extrapolation of our measurements to in vivo neuromodulatory situations must take into account possible problems associated with cell perfusion; nonetheless, our data suggest that basal $I_{to}$ has not been modified by intracellular perfusion.

Frequency-dependent modulation of $I_{to}$ could also contribute to action potential configuration changes with alterations in heartbeat (Binah, 1990). However, due to its relatively rapid recovery kinetics, $I_{to}$ in ferret right ventricle would have a much less pronounced effect on frequency-dependent action potential configuration changes than would the much more slowly recovering $I_{to}$ observed in some other species (e.g., rabbit atrium: Clark et al., 1988; Giles and Imaizumi, 1988). In addition, applying protocols similar to those described by Clark et al. (1988), we did not observe the phenomenon of cumulative inactivation (Qu, Y., and D. L. Campbell, unpublished observations), a property displayed by $I_{to}$ in rabbit atrium (Clark et al., 1988; cf. Aldrich, 1981; DeCoursey, 1990). Finally, the large apparent $Q_{10}$ of

inactivation (10.62, 12–22°C) would suggest that the influence of $I_{to}$ in later stages of repolarization may depend critically on the preparation temperature. This may be one basis for the wide variability in reported characteristics of $I_{to}$ in different cardiac myocytes.

In conclusion, our data demonstrate the presence of a $K^+$-selective, $Ca^{2+}$-independent $I_{to}$ in ferret right ventricular myocytes with kinetics that are appropriate for it to be importantly involved in modulation of phase 1 and later phases of action potential repolarization. Our measurements indicate that (*a*) activation of $I_{to}$ occurs with a sigmoid delay, therefore implying the presence of multiple closed states, (*b*) inactivation occurs as a monoexponential process and is complete at depolarized potentials, and (*c*) the channel can proceed to the closed-inactivated state without first entering the open-conducting state, ruling out a strictly coupled inactivation model (cf. DeCoursey, 1990; Patlak, 1991; Hille, 1992). The Hodgkin-Huxley-type $a^3i$ model developed from our analysis (Table I) can successfully reproduce the macroscopic behavior of ferret right ventricular $I_{to}$. However, because Hodgkin-Huxley formalism has been questioned as an accurate biophysical descriptor of channel gating behavior, in Appendix I we present alternative formulations of three different kinetic models as a possible framework for describing $I_{to}$ gating behavior.

## APPENDIX I: POSSIBLE KINETIC MODELS OF $I_{to}$ CHANNEL INACTIVATION

### *Model 1: Hodgkin-Huxley Type*

The Hodgkin-Huxley (HH) type $a^3i$ formalism developed here for ferret $I_{to}$, and as summarized by the equations in Table I, can be converted into an equivalent linear eight-state Markov model as follows (cf. Hille, 1978, 1992; Armstrong, 1981):

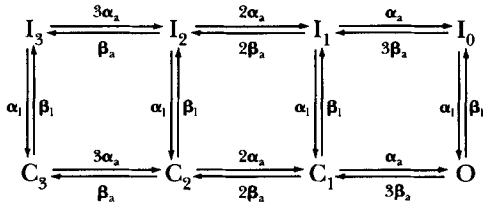


Model 1

where C denotes closed, I denotes inactivated, and O denotes open states of the channel. Model 1 is consistent with and quantitatively reproduces the observed macroscopic $I_{to}$ behavior. As a biophysical descriptor of $I_{to}$ channel behavior at the molecular level, model 1 is based on several important assumptions, including the following: (*a*) activation is composed of three identical and independent processes or gates; (*b*) activation and inactivation are independent processes; and (*c*) inactivation has a strong intrinsic voltage dependence. However, several lines of evidence obtained primarily from *Drosophila* suggest that HH-like formalism is not strictly

applicable at the molecular level for inactivating $K^+$ currents (Solc and Aldrich, 1990; Hoshi, Zagotta, and Aldrich, 1990; for review see Miller, 1991; Jan and Jan, 1992; Zagotta and Aldrich, 1990; Zagotta, Hoshi, and Aldrich, 1990; Bezanilla et al., 1991).

*Model 2*

Zagotta and Aldrich (1990) have presented a model of the rapidly inactivating *Shaker* $A_1$-type channel in cultured embryonic *Drosophila* myotubes which differs from the HH-type model 1 of cardiac $I_{to}$ in the following respects: (*a*) voltage-dependent activation is sigmoid and consists of a series of four steps corresponding to four identical, independent subunits; (*b*) the open state is a bursting state; and (*c*) rapid inactivation is partially coupled to activation and has no intrinsic voltage dependence.

Bursting behavior of ferret ventricular $I_{to}$ channels is likely; our single-channel recordings show a small amplitude current that is noisier than the closed state. Unfortunately, we are unable to quantify these transitions. Since both macroscopic currents and ensemble averages of single $I_{to}$ channels decay as a single exponential, an appropriate modeling approximation is to combine the brief open and closed states that comprise the bursting state into a single aggregate open state. Using this approximation, we can consider the following model:

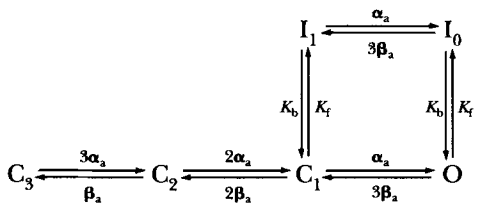


Model 2

where $\alpha_a$ and $\beta_a$ are activation rate constants, while $K_f$ and $K_b$ are voltage-insensitive rate constants for inactivation. For consistency with our measurements, $K_f$ was assumed to be 28.3 $s^{-1}$ (which is the saturating inactivation rate we measured at depolarized potentials; Fig. 10 *B*). Because $I_{to}$ inactivation was experimentally determined to be complete, i.e., residual current was $<2.5\%$ of the fully activated current, $K_b$ was assumed to be 40 times slower than $K_f$ (cf. Zagotta and Aldrich, 1990). An important feature of this model is that all inactivatable states have the same affinity for the putative inactivation particle. Activation merely alters the availability of the channel for inactivation. Model 2 closely mimics the macroscopic conductance produced by HH-type model 1 at depolarized potentials and reproduces the potential dependence of the experimentally observed $I_{to}$ steady-state inactivation relationship as well as the time constants of inactivation at depolarized potentials ($\geq -10$ mV). However, model 2 fails to reproduce recovery from inactivation after a repolarizing step; i.e., recovery proceeds far too slowly due to the rate-limiting nature of $K_b$ compared with that observed experimentally and also fails to reproduce the voltage dependence of recovery observed in the hyperpolarized range of potentials.

*Model 3*

The problem of reconciling voltage-insensitive inactivation with relatively rapid voltage-dependent recovery from inactivation has been addressed in the case of the TTX-sensitive $Na^+$ channel. A partially coupled $Na^+$ channel model has been proposed to account for both voltage-insensitive inactivation and gating current charge immobilization (reviewed in Patlak, 1991). In this model, the apparent voltage dependence of recovery arises from conformational changes associated with the deactivation process: in response to membrane repolarization, one or more of the activation subunits moves back toward the resting state and pushes the inactivation gating particle off or out of its channel binding site. Patlak (1991) has modeled this push-off recovery mechanism for the $Na^+$ channel by inclusion of an additional step between the inactivated and preactivated states (in model 2 this would correspond to including an additional voltage-dependent transition between $I_1$ and $C_2$). To incorporate this mechanism into a characterization of ferret $I_{to}$, we have included an additional inactivated state as follows:

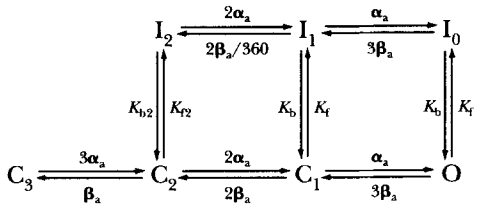


Model 3

In Model 3, $I_2$ differs from both $I_1$ and $I_o$, in that $I_2$ can rapidly undergo transition to $C_2$, but the reverse transition ($C_2$ to $I_2$) has a high energy barrier. In other words, $I_1$ and $I_o$ correspond to high-affinity states for the putative inactivation gating ball, while $I_2$ would correspond to a low-affinity state. To maintain thermodynamic reversibility, the deactivation rate constant $\beta$ was slowed, consistent with the proposal that additional energy is required to push off the inactivation gating particle. The parameters for this model are identical to those previously used for model 2. The additional transitions $K_{f2}$ and $K_{b2}$ are 28.3 $s^{-1}$ and 255 $s^{-1}$, respectively. The transitions between $I_2$ and $I_1$ are $2\alpha_a$ and $2\beta_a/360$.

Model 3 also successfully reproduces both inactivation of $I_{to}$ at depolarized potentials and steady-state inactivation. However, in contrast to model 2, model 3 can reproduce the time dependence of recovery of $I_{to}$ recorded at −70 mV. However, our present formulation of model 3 predicts a stronger voltage dependence of recovery than that which is experimentally observed. We do not consider this to be a serious or inherent limitation of model 3 because the steep voltage dependence of recovery predicted by model 3 results from our unverified assumptions (see below) concerning the exponential nature of $\beta_a$ (e.g., $\beta_a$ may saturate somewhere within the potential range +10 to −90 mV). Finally, although in model 3 inactivation interacts with the open state and the two preceding closed states, we wish to emphasize that, with

appropriate values of $\alpha$, $\beta$, $k_f$, and $k_b$, interaction with one, two, or three preceding closed states is possible. Ultimately, the distinction between such models must rely on gating current measurements.

## APPENDIX II: SOURCES OF BIAS AND UNCERTAINTY IN ANALYSIS OF ACTIVATION

Because the degree of completeness of inactivation was a possible source of systematic bias in our parameter estimation routines, fixed $n = 3$ $I_{to}$ waveforms were simulated using model 3, which produces incomplete inactivation ranging between 12% at 0 mV and 2.9% at +50 mV (expressed as a percentage of peak $I_{to}$). These values compare well with the residual current measured from single-channel ensemble averages (6.8% of peak at the threshold of activation to 3.0% at approximately +50 mV depolarized from threshold). Incomplete inactivation caused a slight systematic overestimation of $n$ from 10% at +10 mV to 2% at +70 mV. This error was in the wrong direction to effect rejection of $n = 4$ and was not of sufficient magnitude to alter rejection of $n = 2$.

To evaluate the 90% rise time criterion, we simulated $I_{to}$ using an HH-type model (model 1) with a fixed activation power of $n = 3$. Simulated fixed $n = 3$ $I_{to}$ waveforms were generated in response to simulated voltage clamp pulses (HP = −70 mV, $V_{pulse}$ = +10 to +70 mV) having an exponential rise time ($\tau$ = 1.4 ms) and analyzed using our standard fitting procedures. Application of the 90% criterion caused a slight underestimation of the actual value of $n = 3$ by no more than 5%, with values ranging from $n = 2.84$ at +10 mV to $n = 2.89$ at +70 mV. In contrast, using the immediate onset of the clamp pulse (i.e., actual $t = 0$ ms) caused an overestimation of the value of $n$ by up to 100%. These simulations suggest that the 90% rise time criterion accurately estimates a value for $n$, subject to the assumptions of independent and identical gating particles. Fitting $I_{to}$ current traces to actual voltage clamp pulse time zero could lead to a serious overestimation of the value of $n$.

Complete kinetic analysis of activation entails measurement of the kinetics of deactivation (i.e., the time constants of tail currents). $I_{to}$ tail currents could be observed in the range 0 to −90 mV (e.g., for $E_{rev}$ measurements), but hyperpolarized to −40 mV tail currents were both small (due to proximity to $E_{rev}$) and rapid (i.e., hard to separate from the capacitive transient). This precluded quantitative analysis of deactivation kinetics in the range of −40 to −90 mV. Unfortunately, in the range where tail currents were better separated from the capacitive transient (−40 to 0 mV), the activation variable $a$ does not assume a zero value. For the HH-like $a^3i$ formulation developed, the tail currents in this range should be composed of at least three closely spaced time constants ($\tau$, $\tau/2$, $\tau/3$; for details, see Hille, 1992). We had little confidence in the ability of numerical fitting procedures to reliably separate and quantitate these components. We therefore assumed that $\alpha_a$ and $\beta_a$ were exponentially dependent on membrane potential (cf. Solc and Aldrich, 1990; Zagotta and Aldrich, 1990).

We wish to acknowledge the technical assistance of Ms. Anne Crews, Ms. Heather McCaslin, and Ms. Steffani Webb.

This work was supported in part by grants from the American Heart Association, North Carolina Affiliate (grant NC 91-G-11) to D. L. Campbell, and the National Institutes of Health (grants 19216, 45132, and 17670) to H. C. Strauss.

*Original version received 8 November 1991 and accepted version received 1 October 1992.*

## REFERENCES

Adams, D. J., S. J. Smith, and S. H. Thompson. 1980. Ionic currents in molluscan soma. *Annual Review of Neuroscience.* 3:141–167.

Aldrich, R. W. 1981. Inactivation of voltage-gated delayed potassium current in molluscan neurons. A kinetic model. *Biophysical Journal.* 36:519–532.

Apkon, M., and J. M. Nerbonne. 1988. Alpha$_1$-adrenergic agonists selectively suppress voltage-dependent $K^+$ currents in rat ventricular myocytes. *Proceedings of the National Academy of Sciences, USA.* 85:8756–8760.

Apkon, M., and J. M. Nerbonne. 1991. Characterization of two distinct depolarization-activated $K^+$ currents in isolated adult rat ventricular myocytes. *Journal of General Physiology.* 97:973–1011.

Armstrong, C. 1981. Sodium channels and gating currents. *Physiological Reviews.* 61:644–683.

Bendorf, K. 1988. Three types of single K channels contribute to the transient outward current in myocardial mouse cells. *Biomedica et Biochimica Acta.* 47:401–416.

Bezanilla, F., E. Perozo, D. M. Papazian, and E. Stefani. 1991. Molecular bases of gating charge immobilization in Shaker potassium channels. *Science.* 254:679–683.

Billette, J., and W. R. Giles. 1991. Electrophysiology of the atrioventricular node: conduction, refractoriness, and ionic currents. *In* Electrophysiology and Pharmacology of the Heart. K. Dangman and D. Miura, editors. Marcel Dekker, Inc., New York. 141–160.

Binah, O. 1990. The transient outward current in mammalian heart. *In* Cardiac Electrophysiology: A Textbook. M. R. Rosen, M. J. Janse, and A. L. Wit, Futura Publishing Company, Inc., Mount Kisco, NY. 93–106.

Braun, A. P., D. Fedida, R. B. Clark, and W. R. Giles. 1990. Intracellular mechanisms for $\alpha_1$-adrenergic regulation of the transient outward current in rabbit atrial myocytes. *Journal of Physiology.* 431:689–712.

Brown, H. F., D. L. Campbell, R. B. Clark, and J. C. Denyer. 1987. Isolated sino-atrial node cells of rabbit: long, thin cells which are calcium-tolerant. *Journal of Physiology.* 390:60P. (Abstr.)

Callewaert, G., J. Vereecke, and E. Carmeliet. 1986. Existence of a calcium-dependent potassium channel in the membrane of cow cardiac Purkinje cells. *Pflügers Archiv.* 406:424–426.

Campbell, D. L., W. R. Giles, K. Robinson, and E. F. Shibata. 1988. Studies of the sodium-calcium exchanger in bull-frog atrial myocytes. *Journal of Physiology.* 403:317–340.

Campbell, D. L., Y. Qu, R. L. Rasmusson, and H. C. Strauss. 1991*a*. Properties of a transient outward $K^+$ current in isolated ferret ventricular myocytes. *Biophysical Journal.* 59:278a. (Abstr.)

Campbell, D. L., Y. Qu, R. L. Rasmusson, and H. C. Strauss. 1991*b*. The transient outward potassium current in isolated ferret right ventricular myocytes: a quantitative kinetic analysis. *Circulation* (Suppl. II) 84:II-103. (Abstr.)

Campbell, D. L., Y. Qu, R. L. Rasmusson, and H. C. Strauss. 1993. The calcium-independent transient outward potassium current in isolated ferret right ventricular myocytes. II. Closed state reverse use-dependent block by 4-aminopyridine. *Journal of General Physiology.* 101:603–626.

Campbell, D. L., R. L. Rasmusson, and H. C. Strauss. 1991*c*. Electrophysiology of the sinus node: ionic and cellular mechanisms underlying primary cardiac pacemaker activity. *In* Electrophysiology and Pharmacology of the Heart. K. Dangman and D. Miura, editors. Marcel Dekker, Inc., New York. 59–108.

Campbell, D. L., R. L. Rasmusson, and H. C. Strauss. 1992. Ionic current mechanisms generating vertebrate primary pacemaker activity at the single cell level: an integrative view. *Annual Review of Physiology.* 54:279–302.

Castle, N. A. 1992. Identification of two distinct $K^+$ currents activated by depolarization in rat ventricular myocytes. *Biophysical Journal.* 61:A307. (Abstr.)

Clark, R. B., W. R. Giles, and Y. Imaizumi. 1988. Properties of the transient outward current in rabbit atrial cells. *Journal of Physiology.* 405:147–168.

Cole, K. S., and J. W. Moore. 1960. Potassium ion current in the squid giant axon. Dynamic characteristic. *Biophysical Journal.* 1:1–14.

Connor, J., and C. F. Stevens. 1971. Voltage clamp studies of a transient outward membrane current in gastropod neural somata. *Journal of Physiology.* 213:21–30.

Dangman, K. 1991. Electrophysiology of the Purkinje fiber. *In* Electrophysiology and Pharmacology of the Heart. K. Dangman and D. Miura, editors. Marcel Dekker, Inc., New York. 161–198.

DeCoursey, T. E. 1990. State-dependent inactivation of $K^+$ currents in rat type II alveolar epithelial cells. *Journal of General Physiology.* 95:617–646.

Denyer, J., and H. F. Brown. 1990. Rabbit sino-atrial node cells: isolation and electrophysiological properties. *Journal of Physiology.* 428:405–424.

Duchatelle-Gourdon, I., H. C. Hartzell, and A. A. Lagrutta. 1988. Modulation of the delayed rectifier potassium current in frog cardiomyocytes by β-adrenergic agonists and magnesium. *Journal of Physiology.* 415:251–274.

Dukes, I. D., and M. Morad. 1991. The transient $K^+$ current in rat ventricular myocytes: evaluation of its $Ca^{2+}$ and $Na^+$ dependence. *Journal of Physiology.* 435:395–420.

Escande, D., A. Coulombe, J. F. Faivre, E. Deroubaix, and E. Coraboeuf. 1987. Two types of transient outward currents in adult human atrial cells. *American Journal of Physiology.* 252:H142–H148.

Fedida, D., Y. Shimoni, and W. R. Giles. 1990. Alpha-adrenergric modulation of the transient outward current in rabbit atrial myocytes. *Journal of Physiology.* 423:257–277.

Gabella, G. 1978. Inpocketings of the cell membrane (caveolae) in the rat myocardium. *Journal of Ultrastructural Research.* 65:135–147.

Giles, W. R., and Y. Imaizumi. 1988. Comparison of potassium currents in rabbit atrial and ventricular cells. *Journal of Physiology.* 405:123–145.

Giles, W. R., and A. C. van Ginneken. 1985. A transient outward current in isolated cells from the crista terminalis of rabbit heart. *Journal of Physiology.* 368:243–264.

Gintant, G. A., I. S. Cohen, N. B. Datyner, and R. P. Kline. 1991. Time-dependent outward currents in the heart. *In* The Heart and Cardiovascular System: Scientific Foundations. 2nd ed. H. A. Fozzard, E. Haber, R. B. Jennings, A. M. Katz, and H. E. Morgan, editors. Raven Press, Ltd., New York. 1121–1169.

Goldman, D. E. 1943. Potential, impedance, and rectification in membranes. *Journal of General Physiology.* 27:37–60.

Gotoh, Y., Y. Imaizumi, M. Watanabe, E. F. Shibata, R. B. Clark, and W. R. Giles. 1991. Inhibition of transient outward $K^+$ current by DHP $Ca^{2+}$ antagonists and agonists in rabbit cardiac myocytes. *American Journal of Physiology.* 260:H1737–H1742.

Hamill, O. P., A. Marty, E. Neher, B. Sakmann, and F. J. Sigworth. 1981. Improved patch clamp techniques for high-resolution current recording from cell and cell-free membrane patches. *Pflügers Archiv.* 391:85–100.

Harvey, R. D., and R. E. Ten Eick. 1988. Characterization of the inward-rectifying potassium current in cat ventricular myocytes. *Journal of General Physiology.* 91:593–615.

Hille, B. 1978. Ionic channels in excitable membranes. Current problems and biophysical approaches. *Biophysical Journal.* 22:283–294.

Hille, B. 1992. Ionic Channels of Excitable Membranes. 2nd ed. Sinauer Associates, Inc., Sunderland, MA. 607 pp.

Hiraoka, M., and S. Kawano. 1989. Calcium-sensitive and insensitive transient outward current in rabbit ventricular myocytes. *Journal of Physiology.* 410:187–212.

Hodgkin, A. L., and A. F. Huxley. 1952. A quantitative description of membrane current and its application to conduction and excitation in nerve. *Journal of Physiology.* 117:500–544.

Hodgkin, A. L., and B. Katz. 1949. The effect of sodium ions on the electrical activity of the giant axon of the squid. *Journal of Physiology.* 108:37–77.

Hondeghem, L. M., and D. J. Snyders. 1990. Class III antiarrhythmic agents have a lot of potential but a long way to go: reduced effectiveness and dangers of reverse use dependence. *Circulation.* 81:686–690.

Hoshi, T., W. N. Zagotta, and R. W. Aldrich. 1990. Biophysical and molecular mechanisms of Shaker potassium channel inactivation. *Science.* 250:533–538.

Hume, J. R., W. Giles, K. Robinson, E. F. Shibata, R. D. Nathan, K. Kanai, and R. Rasmusson. 1986. A time- and voltage-dependent K current in single cardiac cells from bullfrog atrium. *Journal of General Physiology.* 88:777–798.

Hume, J. R., A. Uehara, R. W. Hadley, and R. D. Harvey. 1990. Comparison of $K^+$ channels in mammalian atrial and ventricular myocytes. *In* Potassium Channels: Basic Function and Therapeutic Aspects. T. J. Colatsky, editor. Alan R. Liss, Inc., New York. 17–41.

Imaizumi, Y., and W. R. Giles. 1987. Quinidine-induced inhibition of transient outward current in cardiac muscle. *American Journal of Physiology.* 253:H704–H708.

Jan, L. Y., and Y. N. Jan. 1992. Structural elements involved in specific $K^+$ channel functions. *Annual Review of Physiology.* 54:537–555.

Josephson, I. R., J. Sanchez-Chapula, and A. M. Brown. 1984. Early outward current in rat single ventricular cells. *Circulation Research.* 54:157–162.

Koren, G., E. R. Liman, D. E. Logothetis, B. Nadal-Ginard, and P. Hess. 1990. Gating mechanism of a cloned potassium channel expressed in frog oocytes and mammalian cells. *Neuron.* 2:39–51.

Lefevre, I., A. Coulombe, and E. Coraboeuf. 1991. The calcium antagonist D600 inhibits calcium-independent transient outward current in isolated rat ventricular myocytes. *Journal of Physiology.* 432:65–80.

MacKinnon, R. 1991. Determination of the subunit stoichiometry of a voltage-activated potassium channel. *Nature.* 350:232–235.

Marty, A., and E. Neher. 1983. Tight-seal whole-cell recording. *In* Single-Channel Recording. B. Sakmann and E. Neher, editor. Plenum Publishing Corp., New York. 107–122.

Miller, C. 1991. 1990: Annus mirabilis of potassium channels. *Science.* 252:1092–1096.

Nakayama, T., and H. Irisawa. 1985. Transient outward current carried by potassium and sodium in quiescent atrioventricular node cells of rabbits. *Circulation Research.* 57:65–73.

Nathan, R. D. 1986. Two electrophysiologically distinct types of cultured pacemaker cells from rabbit sinoatrial node. *American Journal of Physiology.* 250:H325–H329.

Neher, E. 1971. Two fast transient current components during voltage clamp in snail neurons. *Journal of General Physiology.* 58:36–53.

Patlak, J. 1991. Molecular kinetics of voltage-dependent $Na^+$ channels. *Physiological Reviews.* 71:1047–1080.

Pennefather, P., and I. S. Cohen. 1990. Molecular mechanisms of cardiac $K^+$ channel regulation. *In* Cardiac Electrophysiology: From Cell to Bedside. D. Zipes and J. Jalife, editors. W.B. Saunders Co., Philadelphia. 17–28.

Qu, Y., D. L. Campbell, H. H. Himmel, and H. C. Strauss. 1992. ATP reduces L-type $I_{Ca}$ independently of $Ca^{2+}$-dependent inactivation in ferret ventricular myocytes. *Biophysical Journal.* 61:400a. (Abstr.)

Qu, Y., D. L. Campbell, A. R. Whorton, and H. C. Strauss. 1991. Modulation of $I_{Ca}$ by ATP in ferret right ventricular myocytes. *Circulation.* 84:II-172. (Abstr.)

Rudy, B. 1988. Diversity and ubiquity of K channels. *Neuroscience.* 25:729–749.

Sanguinetti, M. C. 1990. $Na_i^+$-activated and ATP-sensitive $K^+$ channels in the heart. *In* Potassium Channels: Basic Function and Therapeutic Aspects. T. J. Colatsky, editor. Alan R. Liss, Inc., New York. 85–109.

Sanguinetti, M. C., and N. K. Jurkiewicz. 1990. Two components of cardiac delayed rectifier $K^+$ current. Differential sensitivity to block by class III antiarrhythmic agents. *Journal of General Physiology.* 96:195–215.

Shibata, E. F., T. Drury, H. Refsum, V. Aldrete, and W. Giles. 1989. Contributions of a transient outward current to repolarization in human atrium. *American Journal of Physiology.* 257:H1773–H1781.

Solc, C. K., and R. W. Aldrich. 1990. Gating of single non-Shaker A-type potassium channels in larval *Drosophila* neurons. *Journal of General Physiology.* 96:135–165.

Solc, C. K., W. N. Zagotta, and R. W. Aldrich. 1987. Single-channel and genetic analyses reveal two distinct A-type potassium channels in *Drosophila. Science.* 236:1094–1098.

Sorota, S. 1992. Swelling-induced chloride-sensitive current in canine atrial cells revealed by whole-cell patch-clamp method. *Circulation Research.* 70:679–687.

Sorota, S., and P. Boyden. 1991. Electrophysiology of the atrial myocardium. *In* Electrophysiology and Pharmacology of the Heart. K. Dangman and D. Miura, editors. Marcel Dekker, Inc., New York. 109–139.

Tseng, G. N., and B. F. Hoffman. 1989. Two components of transient outward current in canine ventricular myocytes. *Circulation Research.* 64:633–647.

Vandenberg, C. A., and F. Bezanilla. 1991. A sodium channel gating model based on single channel, macroscopic ionic, and gating currents in the squid giant axon. *Biophysical Journal.* 60:1511–1533.

Wasserstrom, J. A., and R. E. Ten Eick. 1991. Electrophysiology of mammalian ventricular muscle. *In* Electrophysiology and Pharmacology of the Heart. K. Dangman and D. Miura, editors. Marcel Dekker, Inc., New York. 199–233.

Zagotta, W. N., and R. W. Aldrich. 1990. Voltage-dependent gating of Shaker A-type potassium channels in *Drosophila* muscle. *Journal of General Physiology.* 95:29–60.

Zagotta, W. N., M. S. Brainard, and R. W. Aldrich. 1988. Single-channel analysis of four distinct classes of potassium channels in *Drosophila* muscle. *Journal of Neuroscience.* 8:4765–4779.

Zagotta, W. N., T. Hoshi, and R. W. Aldrich. 1990. Restoration of inactivation in mutants of Shaker potassium channels by a peptide derived from ShB. *Science.* 250:568–571.